

# Interplay of synergy and redundancy in diamond motif

Ayan Biswas<sup>1, a)</sup> and Suman K Banik<sup>1, b)</sup>

*Department of Chemistry, Bose Institute, 93/1 A P C Road, Kolkata 700009, India*

The formalism of partial information decomposition provides a number of independent components which altogether constitute the total information provided by the source variable(s) about the target variable(s). These non-overlapping terms are recognized as unique information, synergistic information and, redundant information. The metric of net synergy conceived as the difference between synergistic and redundant information, is capable of detecting effective synergy, effective redundancy and, information independence among stochastic variables. The net synergy can be quantified using appropriate combinations of different Shannon mutual information terms. The utilization of the net synergy in network motifs with the nodes representing different biochemical species, involved in information sharing, uncovers rich store for exciting results. In the current study, we use this formalism to obtain a comprehensive understanding of the relative information processing mechanism in a diamond motif and two of its sub-motifs namely bifurcation and integration motif embedded within the diamond motif. The emerging patterns of effective synergy and effective redundancy and their contribution towards ensuring high fidelity information transmission are duly compared in the sub-motifs. Investigation on the metric of net synergy in independent bifurcation and integration motifs are also executed. In all of these computations, the crucial roles played by various systemic time scales, activation coefficients and signal integration mechanisms at the output of the network topologies are especially emphasized. Following this plan of action, we become confident that the origin of effective synergy and effective redundancy can be architecturally justified by decomposing a diamond motif into bifurcation and integration motif. According to our conjecture, the presence of common source of fluctuations creates effective redundancy. Our calculations reveal effective redundancy empowers signal fidelity. Moreover, to achieve this, input signaling species avoids strong interaction with downstream intermediates. This strategy is capable of making the diamond motif noise-tolerant. Apart from the topological features, our study also puts forward the active contribution of additive and multiplicative signal integration mechanisms to nurture effective redundancy and effective synergy.

Keywords: partial information decomposition, information theory, fluctuations, signaling networks

Over the years, the theory of information, as conceptualized by Claude Shannon, has gained much importance in analyzing biological phenomena. As a recent development, partial information decomposition (PID) has been proposed as an extended framework to tackle multivariate information processing, storage and transmission in complex animate systems. As an outcome of PID, one can analyze the total information content of a system by dividing it into a number of non-overlapping information terms of differing and distinct flavors. A multivariate system, therefore, can have unique information, synergistic information and, redundant information. Application of PID in biological systems, till now, is not much and such analysis needs to be undertaken to formalize the nascent framework in perspective. We chose a ubiquitous network motif, namely, a diamond motif to understand the origin of redundant and synergistic information in a signaling channel. Identification and information-theoretic analysis of sub-motifs of the diamond motif, namely, bifurcation motif and integration motif, play a crucial role to satisfactorily answer the question raised by us. The metric of our interest, the net synergy, is computed as the difference in synergistic and redundant information. Here, it is analyzed with respect to variations in a number of significant systemic parameters and reveals essential characteristics of the interlinked information components. We found that effective redundant information is produced when more than one downstream node share a common upstream node. This upstream node acts as a common source of fluctuations for the downstream nodes, thereby causing information sharing. Our computations also reveal that increase in effective redundant information concurrently increases signal-to-noise ratio or the signal fidelity of the information channel. We find that separation of time scales of input and output nodes or components modulates transmission of effective redundant information in the network. In addition to this, the strength with which the upstream component activates its downstream components has to be in the low to moderate spectrum to achieve a significant amount of redundant information. We have cultivated the effect of additive and multiplicative

---

<sup>a)</sup>Electronic mail: ayanbiswas@jcbose.ac.in

<sup>b)</sup>Electronic mail: skbanik@jcbose.ac.in

signal integration mechanisms, which closely approximate the biological realities in well-known gene regulatory networks. It has been found to alter the level of the net synergy throughout biologically plausible parametric settings. As a final step, our study proposes efficient parameter regimes where one of the sub-motifs overpowers its counterpart in contributing the desirable net synergy, in order to be comparatively more noise-tolerant.

## I. INTRODUCTION

To optimise different biophysical processes, in continuous and dynamic interactions with their surroundings, animate systems have to perform numerous and necessary computations. The resulting decisions made by the organisms categorically influence the fitness of the species in the competition for evolutionary selection mechanisms<sup>1–14</sup>. To identify the governing physical principles that the species are constrained to obey in order to achieve adaptability in a fluctuating environment, sophisticated measures arising from information theory<sup>9,15–17</sup> have been proven to be logistically handy as well as predictive<sup>3,8,10–12,18–28</sup>. These optimizing physical principles often dictate the organism to opt for certain distinctive architectural complexity<sup>1,29,30</sup>. The investigation regarding the connection between the topological features of recurrent biological motifs and efficient information processing does not require detailed knowledge of the architectural details of the model system. This is because information theory deals with the biological motif as a signal communication system consisting message transmitting source, receiver at the output point and the intermediate signal propagation pathway. This pathway may be regarded as a black box where the noise comes in to corrupt the purity of the transmitted message<sup>15,31</sup>.

Diamond motif (DM) is one of the recurring biological patterns<sup>29,32,33</sup> and is interesting on a number of counts. It is one of the two prominent four node motifs found in signal transduction networks, the other being the bi-fan. Surprisingly, DM (initially known as Bi-parallel<sup>29</sup>) is found in diverse networks, e.g. in neuronal networks of *C. elegans*, ecological food webs and in forward logic chips embedded in electronic circuits<sup>29,32,33</sup>. DM is generalized as multiple layered perceptrons found in the neural network of *C. elegans*<sup>32</sup>. One can decompose the DM into combinations of various sub-motifs and discuss the arising advantage points. We know one such prominent attempt using information-theoretic analysis where the authors dissected the DM into two two-step cascade (TSC) motifs and characterized profiles of gain, noise and the gain-to-noise ratio<sup>34</sup>. In that paper, DM is evoked in the perspective of multimerization and their analysis shows the emergence of a band-pass filter type behavior of DM. One of their key conclusions suggested that network performance is independent of its architectural features and can be manipulated by modification of inter-species coupling strengths. Another approach has identified DM as a generalization of incoherent feed-forward loop motif and the results showed its band-pass filter type response to signal with temporal periodicity<sup>35</sup>. It should be noted here that the analysis performed in the existing literature<sup>34,35</sup> used biologically plausible parameters due to non-availability of experimental data.

In the present communication, we have looked into the problem of efficient information processing in the DM from a fresh perspective. One can think of constructing DM using independent bifurcation motif (BM) and independent integration motif (IM). It is also possible to identify two different sub-motifs embedded in DM, namely bifurcation sub-motif (BM-DM) and integration sub-motif (IM-DM) (see Fig. 1). We have adopted an information-theoretic measure which involves a suitable combination of three-variable and two-variable mutual information (MI) terms and the combination is known as the net synergy<sup>36,37</sup>. It has the potential to predict synergy, redundancy and, information independence among stochastic variables involved in information processing in a complex system. The net synergy is a product of partial information decomposition (PID)<sup>37,38</sup>. Using PID, we can decompose the total information provided by a set of source variables about a target variable into independent or non-overlapping information terms namely unique information, synergistic information and, redundant information. Unique information is the information about the target variable provided only by a specific source variable whereas redundant information about the target is provided by all the source variables holding common shares. Synergistic information about the target is provided jointly by the set of source variables. In other words, to get hold of the synergistic information about a target variable, one has to know all the source variables simultaneously. As mentioned by Barrett<sup>37</sup>, for a system of three random variables, one can link three MI terms with four information terms generated through PID (i.e. two unique information, synergistic information and, redundant information) using only three equations. Four unknown PID terms related through three equations make the system under-specified in the absence of any specific definition for any one of the unknowns. Hence, from this system of equations, only the difference between synergistic information and redundant information (i.e. the net synergy) may be obtained<sup>37</sup>. The positive value of net synergy implies that synergy is dominant over redundancy. For negative values of the net synergy, redundancy overpowers synergy. The borderline case of zero net synergy indicates information independence among information source and target variables<sup>36,37</sup>.

There exists rich literature on multivariate information decomposition which is an active field of research. For a

comparative discussion on different measures involving multivariate information along with their applications, the review by Timme *et. al.*, is notable<sup>39</sup>. In a broader perspective, Faes *et. al.*, have been able to show that computation of information storage and its transfer are necessary to predict the dynamics of target variable<sup>40</sup>. Synergistic and redundant information transfer components have been exactly computed for coupled Gaussian systems operating across multiple time scales<sup>41</sup>. It has been also pointed out that the questions regarding definitions of what constitutes synergy and redundancy in case of nonlinear systems are at present not satisfactorily settled<sup>41</sup>. Apart from information storage and transfer, Ref. 42, directs our attention to assemble information modification formalism to better understand dynamics of complex network topologies. Besides, composite analysis of information-dynamic measures can underpin the causal effects that follow from the dynamics which itself is susceptible to varying experimental conditions<sup>43</sup>. In a study performed by Bertschinger *et. al.*, measures have been proposed for decompositions of multivariate MI-s along with a working concept for the unique information<sup>44</sup>. Different quantifiers of synergistic information have been applied in a set of binary circuits for their comparative analysis<sup>45</sup>. For a new formalism regarding redundant information and its usage to decompose transfer entropy, one can take note of the proposal by Harder *et. al.*,<sup>46</sup>. Recent findings according to Wibral and colleagues have projected PID as a consistent framework such that it can compare different neural goal functions and formulate potential new candidates<sup>47</sup>. To supplement advances in theoretical understanding on multivariate information decomposition, experimentalists have also contributed their fair share in this ever-growing research domain. Gawne and Richmond have experimented on synergistic, redundant and, independent information encoding inside the inferior temporal cortex region in behaving rhesus monkey brain<sup>48</sup>. The role played by correlations in the encoding mechanisms inside the nervous system has also been central to elaborate and thought-provoking research<sup>49</sup>. Brenner *et. al.*, demonstrated that even the motion stimulated visual information processing device of a fly uses synergistic code<sup>50</sup>. Analytical study utilizing information theory and focussing on the importance of correlations related to somatosensory cortical populations in rats can be found in Ref. 51. This interesting paper has presented the fact that to actually explain their experimental data, it is indeed important to consider correlational order greater than two.

In the present work, we have not attempted any extension or modification of the existing formalism of PID. Instead, we have a clear objective to apply PID to study information processing in a ubiquitous gene regulatory network (GRN) motif, i.e. DM. Barrett<sup>37</sup> has studied some example cases of dynamical systems having biological analogs, but the processes are modeled as of multivariate autoregressive nature. It makes the time-evolution of the system discrete and the interactions linear, which are seldom shown by living systems. We envisaged the situation quite the opposite, i.e. a system with continuous temporal variations and nonlinear interactions. The discreteness in time is brought by the author to showcase the effect of past states of the source variables on the future state of the target variable. However, here we are concerned with the net synergy aspects where all the variables are at the same time point, i.e. without any time-lag.

The role of redundancy to combat noise in the information channel was previously presented by Shannon and Weaver in their illuminating book<sup>52</sup> which motivated us to look for analogs in model network motifs. The theoretical explanation regarding the origin of redundancy in a two-step cascade motif and its connection with information fidelity have been discussed thoroughly in our earlier work<sup>53</sup>. In Ref. 54, authors have presented a case of redundancy where multiple genes with successively higher values of activating signal strengths, are driven by a single input. Another interesting recent study has found out that genetic redundancy along with intrinsic noise and heterogeneity can increase information transfer whereas extrinsic noise and cross-talk have an inverse effect<sup>55</sup>. Immunofluorescence readouts from network experiments involving NF- $\kappa$ B and ATF-2 receiving the signal from tumor necrosis factor (TNF) through TNF receptor, reveal the mitigation of noisy effects. Thus information propagation is enhanced with the help of redundancy<sup>23</sup>. Rhee and colleagues have been successful in detecting connections between network architecture and associated noise of biochemical origin<sup>56</sup>. Whereas these studies have reported the connection between information fidelity and redundancy (architectural or/and informational), our analysis has quantified this connection in model network motif with a strong emphasis on PID. Moreover, in our current initiative, attempts have been made to showcase the connection between network topology and the synergy-redundancy duo. Also, to be specific, this line of analysis qualifies as being the central theme of the present report.

To this end, we have chosen signal-to-noise ratio (SNR) as the measure of fidelity<sup>26,53</sup> in the motifs. Gain-to-noise ratio (GNR) plays another strong candidate which can successfully quantitate the performance of the network motif, and it does so independently of the signal characteristics<sup>22</sup>. One can also link GNR to the Fisher information about the signaling species provided by the output species or response<sup>16,22</sup>. The analysis performed here has been done at steady states of involved species as it is suggested that living systems perform optimally in their steady states and keeping concentrations or copy numbers fixed helps to compare different parametric scenarios on an equal footing<sup>32</sup>. Additionally since in our case, the signaling species driving the DM follows Poisson process, SNR is found to be proportional to GNR. Here, the steady state ensemble averaged population of the signaling species serves as the constant factor of proportionality.

We have used the relaxation time scale as a parameter because the separation of time scale is crucial to dictate

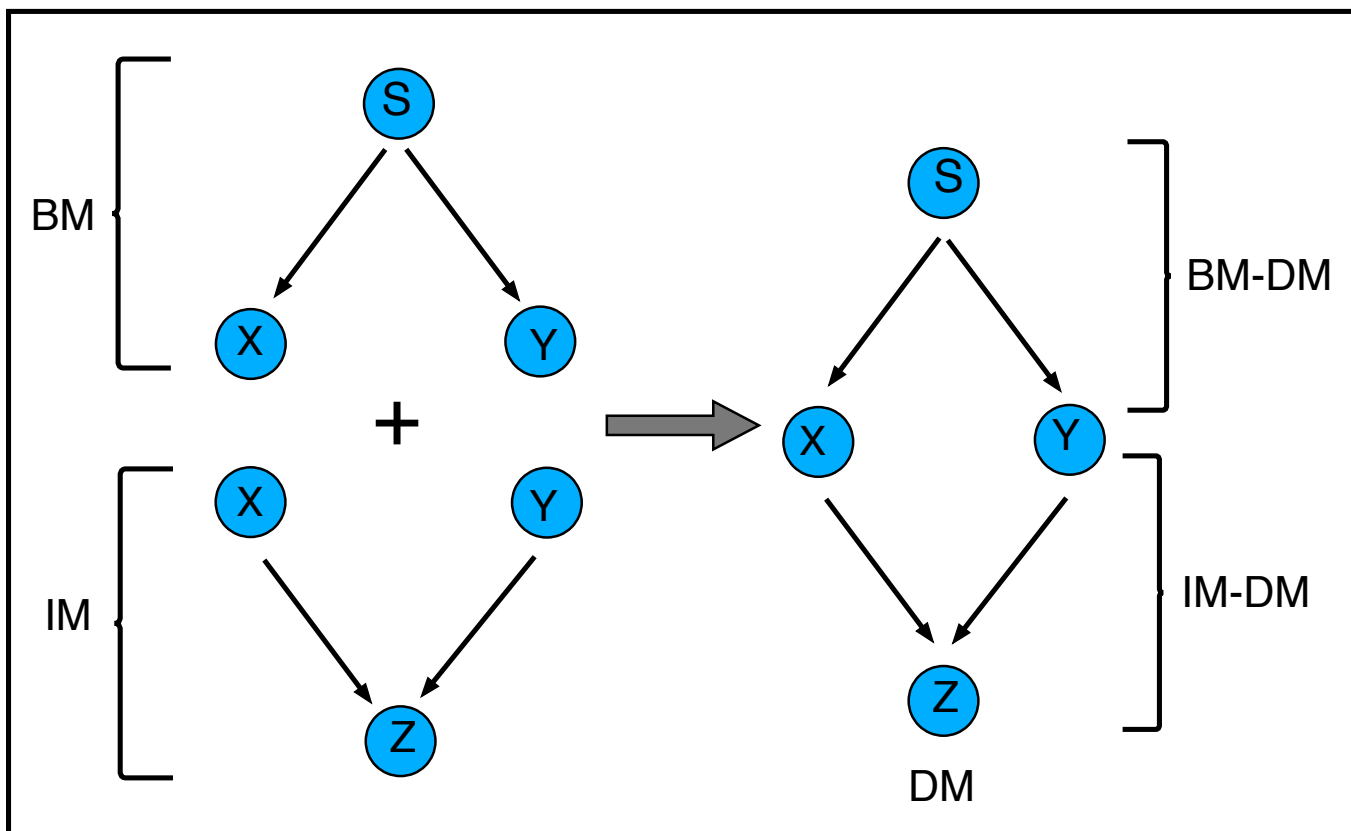


FIG. 1. Schematic diagram of bifurcation motif (BM), integration motif (IM) and diamond motif (DM). BM-DM and IM-DM respectively stands for the bifurcation and integration sub-motif embedded within the diamond motif.

the information flow in a biochemical network behaving like a noise filter<sup>14,22,34,57-59</sup>. To this end, it is important to mention that the biological system's reaction to the input signal is indeed amplitude and frequency dependent. Since, DM and the associated motifs and sub-motifs are the living analogs of an electronic signal processing device, concepts of encoding and decoding can be equivalently mapped to these biological motifs<sup>28,36</sup>. Here, we show that the features of the net synergy landscape of the motifs and sub-motifs are intricately connected to the principles of communication theory.

The response of a transcription control network depends on the mechanism adopted by the organism to integrate multiple incoming signals. For example, in the well-characterized *lac* system of *E. coli*, this integration machinery is intermediate between boolean OR logic and AND logic. By implementing a few point mutations in the system, pure logic such as OR, AND or, single-input switches have been achieved. It implies the plasticity of the *lac* operon's integration function<sup>60,61</sup>. These fundamental discoveries motivated us to investigate how does the signal integration mechanism affect the characteristics of the net synergy profiles and vary the fidelity of signal processing. Though in principle, a significant number of different logic gates can be implemented in synthetic set-ups, evolvability of these modular structures inside living cells is not always guaranteed<sup>62</sup>. In this connection, we find PID to provide some preliminary ideas. For the sake of simplicity, we restrict the input integration mechanism to be either additive or multiplicative, keeping the expression levels of all the biochemical species constant throughout different cases for better comparison.

Some other technical points that the present report takes benefit of are as follows. We have used Gaussian random variables to represent the biochemical species so that we can treat the MI of various channels as their respective channel capacities<sup>22</sup> and these can be easily computed using corresponding variance and covariance. We have made our analysis tractable further by assuming Gaussian noise processes<sup>4,20,22,53,57,59,63-67</sup>. We use noise with zero cross-correlation, because biological phenomenology dictates the validity of this approach in a birth-death type of dynamics<sup>34</sup>, as dealt here. Another vital point to note here is the consideration of low copy number<sup>4,7,54,68,69</sup> of the biochemical species involved in the stochastic reactions.

We performed the theoretical analysis using linear noise approximation (LNA)<sup>63,64,67,70-72</sup> to handle nonlinearity

which enters into the system through the Hill type regulatory functions<sup>20,54,73-75</sup> used in our mathematical model. We do take note of the fact that there are other techniques, e.g. the small-noise approximation that can be applied to tackle the fluctuations in the system<sup>54,76</sup>. Though low copy numbers of the reacting molecules contribute a significant amount of noise into the reaction volume, a good match between our analytical results and stochastic simulations based on Gillespie's method<sup>77,78</sup> establishes the validity of LNA. In this connection, our observations receive strong support from previous findings of similar type considering copy number as low as  $\sim 10$ .<sup>20,53,57,59</sup> From current literature<sup>67</sup>, LNA is known to be effective beyond high copy number reactions. It gives out exact results up to the second moments of the system components involved in second-order reactions. There may be a number of species that are involved in these specific type of reactions, but it is noted that at least one of those reacting species in every such reaction fluctuates not only in a Poissonian way but also in an uncorrelated fashion with the rest of the species<sup>67</sup>.

## II. THE MODEL

The set of Langevin equations governing the dynamics of a DM are,

$$\frac{ds}{dt} = f_s(s) - \mu_s s + \xi_s(t), \quad (1)$$

$$\frac{dx}{dt} = f_x(s, x) - \mu_x x + \xi_x(t), \quad (2)$$

$$\frac{dy}{dt} = f_y(s, y) - \mu_y y + \xi_y(t), \quad (3)$$

$$\frac{dz}{dt} = f_z(s, x, y, z) - \mu_z z + \xi_z(t). \quad (4)$$

Here, to represent the copy numbers of species S, X, Y and, Z present in the unit amount of cellular volume, we use the symbols  $s, x, y$  and,  $z$ , respectively. To be precise, if one considers these biochemical species to be transcription factors, the corresponding volume has to be an effective volume since these transcription factors after being produced in the cytoplasm are carried inside the nucleus where they are sensed. Hence merely considering either the cellular or the nuclear volume would be inaccurate<sup>75</sup>. The set of Langevin equations written above is suggestive of birth-death type of mechanisms governing the population levels. We have modelled degradation to be proportional to the respective population size with  $\mu_i$ -s ( $i = s, x, y, z$ ) setting the time scale of degradation. The inter-species interactions are manifested through the synthesis of X, Y and, Z. These terms are taken to be nonlinear, in general, in agreement with real biological scenario<sup>20,34,73,74,76</sup>. In the present analysis we use  $\langle \xi_i(t) \rangle = 0$  and  $\langle \xi_i(t) \xi_j(t') \rangle = \langle |\xi_i|^2 \rangle \delta_{ij} \delta(t-t')$ , which makes the noise processes independent and Gaussian distributed. At steady state the noise strength becomes  $\langle |\xi_i|^2 \rangle = \langle f_i \rangle + \mu_i \langle i \rangle = 2\mu_i \langle i \rangle$  where  $i = s, x, y$  and,  $z$ <sup>63-65,69-71,79,80</sup>. The first equality demonstrates that both synthesis and degradation processes are sources for noise in the system and their individual contributions add up to produce the ultimate steady state noise strength. The second equality indicates that both the noise sources contribute in equal proportions at steady state. The usage of  $\langle \dots \rangle$  denotes steady state ensemble average over many independent realizations. To calculate the second moments of  $s, x, y$  and,  $z$  through LNA, we apply perturbation of linear order  $\delta u(t) = u(t) - \langle u \rangle$  with  $\langle u \rangle$  being the average population of  $u$  at steady state and recast Eqs. (1-4) in the following form

$$\frac{d\delta\mathbf{W}}{dt} = \mathbf{J}_{W=\langle W \rangle} \delta\mathbf{W}(t) + \boldsymbol{\Xi}(t), \quad (5)$$

where we denote by  $\delta\mathbf{W}(t)$ , the fluctuation matrix containing the linear order perturbations and the noise matrix by  $\boldsymbol{\Xi}(t)$

$$\delta\mathbf{W}(t) = \begin{pmatrix} \delta s(t) \\ \delta x(t) \\ \delta y(t) \\ \delta z(t) \end{pmatrix}, \boldsymbol{\Xi}(t) = \begin{pmatrix} \xi_s(t) \\ \xi_x(t) \\ \xi_y(t) \\ \xi_z(t) \end{pmatrix},$$

$\mathbf{J}$  represents the Jacobian matrix at steady state. The Lyapunov equation at steady state<sup>69-71,81,82</sup>

$$\mathbf{J}\boldsymbol{\Sigma} + \boldsymbol{\Sigma}\mathbf{J}^T + \mathbf{D} = \mathbf{0}, \quad (6)$$

establishes connections between the steady-state fluctuations of the biochemical species and noise-driven dissipation in the system. The fluctuation part is encapsulated in  $\boldsymbol{\Sigma}$  which is the covariance matrix, and  $\mathbf{D}$  contains the dissipation part since its entries are various noise strengths, i.e.  $\mathbf{D} = \langle \boldsymbol{\Xi}\boldsymbol{\Xi}^T \rangle$  where  $T$  denotes matrix transposition operation.



In the generalized analytic expressions of the second moments (see Appendix) obtained by solving the Lyapunov equation at steady state,  $s, x, y$  and,  $z$  are approximated as  $\langle s \rangle, \langle x \rangle, \langle y \rangle$  and,  $\langle z \rangle$ , respectively<sup>53,59,63</sup>. These second moments serve as the ingredients for calculating the two-variable and three-variable MI terms. For computing the net synergy (in the unit of ‘bits’) among S, X and, Y which constitute BM and BM-DM, and among X, Y and, Z which constitute IM and IM-DM, we use the following two expressions<sup>28,36–38,53</sup>

$$\Delta I(s; x, y) = I(s; x, y) - I(s; x) - I(s; y), \quad (7)$$

$$\Delta I(z; x, y) = I(z; x, y) - I(z; x) - I(z; y). \quad (8)$$

Here, it is to be kept in mind that information-theoretic characterization of the random variables may not be at par with the causal relations among them<sup>37</sup>. Though S regulates X and Y, which in turn regulate Z, it is feasible to consider X and Y as the information source and S as the information target while computing  $\Delta I(s; x, y)$ . In contrast, we regard X and Y as the information source and Z as the information target to calculate  $\Delta I(z; x, y)$ . The choice of grouping variables into these categories should be dictated by the rationale of the question being asked for specific network architecture. In the framework of Shannon, the network motifs are logically thought of as signal processing channels, and by the same token, the information propagation phenomenon can be described as a joint encoding-decoding process<sup>15,36</sup>.  $\Delta I(s; x, y)$  gets the advantage of the decoding scheme taking the intermediates X and Y as the source of information for S. On the other side, these same intermediates can take part in encoding information and transfer to Z and hence, the relevant net synergy turns out to be  $\Delta I(z; x, y)$ . Specifically in our system, one of the key questions that we want to investigate is how does a common source of fluctuations affect the net synergy landscape. Since the intermediate information hubs X and Y are common nodes in the sub-motifs, one can infer both S (decoding) and Z (encoding) starting with X and Y. We emphasise that the PID induced source-target specifications do not levy any constraint on the chemical kinetics of these species.

According to Ref. 37, synergistic information ( $I_S$ ) and redundant information ( $I_R$ ) constitutes the net synergy  $\Delta I$  as follows

$$\Delta I = I_S - I_R. \quad (9)$$

It is evident from the above equation that positive net synergy ( $\Delta I > 0$ ) reveals a greater amount of synergy in comparison with redundancy while negative net synergy ( $\Delta I < 0$ ) reverses the situation. One should take note of the fact that  $\Delta I > 0$  arises when  $I_S > I_R \geq 0$ , i.e.  $I_R$  may or may not exist but  $I_S$  is sure to exist and is greater in proportion than  $I_R$ . On the other hand,  $\Delta I < 0$  implies  $I_R > I_S \geq 0$ , i.e.  $I_S$  may or may not be there but  $I_R$  is definitely present and is more significant than  $I_S$ . For the sake of clarity, we paraphrase  $\Delta I > 0$  by effective synergy  $I_{ES}$  and  $\Delta I < 0$  by effective redundancy  $I_{ER}$ . Synergy and redundancy can also balance each other, and this gets reflected in zero amount of the net synergy ( $\Delta I = 0$ ). This situation demands  $I_S = I_R \geq 0$ , i.e. either both  $I_S$  and  $I_R$  exist in equal proportion or both are absent. One should be mindful about these conceptual points while analyzing the net synergy profiles generated with respect to variations of different system parameters and should not be led to infer that any attempt to quantify absolute synergy and absolute redundancy has been made. The existence of pure synergy and pure redundancy have been speculated entirely based upon the qualitative nature of synergistic and redundant information due to the framework of PID.

Also, one should not conclude based on the source-target classifications and the polarity of the net synergy that these metrics provide directionality of information flow. MI is a sophisticated and generalized measure of correlation, and it is strictly semi-positive. The net synergy also captures correlation more finely with respect to information independence of the associated random variables<sup>36</sup>. Besides, correlation does not infer causation. For that matter, since we are considering a directed network, the direction of information flow is entirely determined by the specified interactions. Now, for Gaussian random variables, Eqs. (7-8) become<sup>37</sup>

$$\begin{aligned} \Delta I(s; x, y) = & \frac{1}{2} \left( \log_2 \left[ \frac{\det \Sigma(s)}{\det \Sigma(s|x, y)} \right] - \log_2 \left[ \frac{\det \Sigma(s)}{\det \Sigma(s|x)} \right] \right. \\ & \left. - \log_2 \left[ \frac{\det \Sigma(s)}{\det \Sigma(s|y)} \right] \right), \end{aligned} \quad (10)$$

$$\begin{aligned} \Delta I(z; x, y) = & \frac{1}{2} \left( \log_2 \left[ \frac{\det \Sigma(z)}{\det \Sigma(z|x, y)} \right] - \log_2 \left[ \frac{\det \Sigma(z)}{\det \Sigma(z|x)} \right] \right. \\ & \left. - \log_2 \left[ \frac{\det \Sigma(z)}{\det \Sigma(z|y)} \right] \right). \end{aligned} \quad (11)$$

The consecutive terms in the right-hand side of Eq. (10) denote  $I(s; x, y)$ ,  $I(s; x)$  and,  $I(s; y)$ , respectively. Similarly, the consecutive terms in the right-hand side of Eq. (11) denote  $I(z; x, y)$ ,  $I(z; x)$  and,  $I(z; y)$ , respectively. The terms

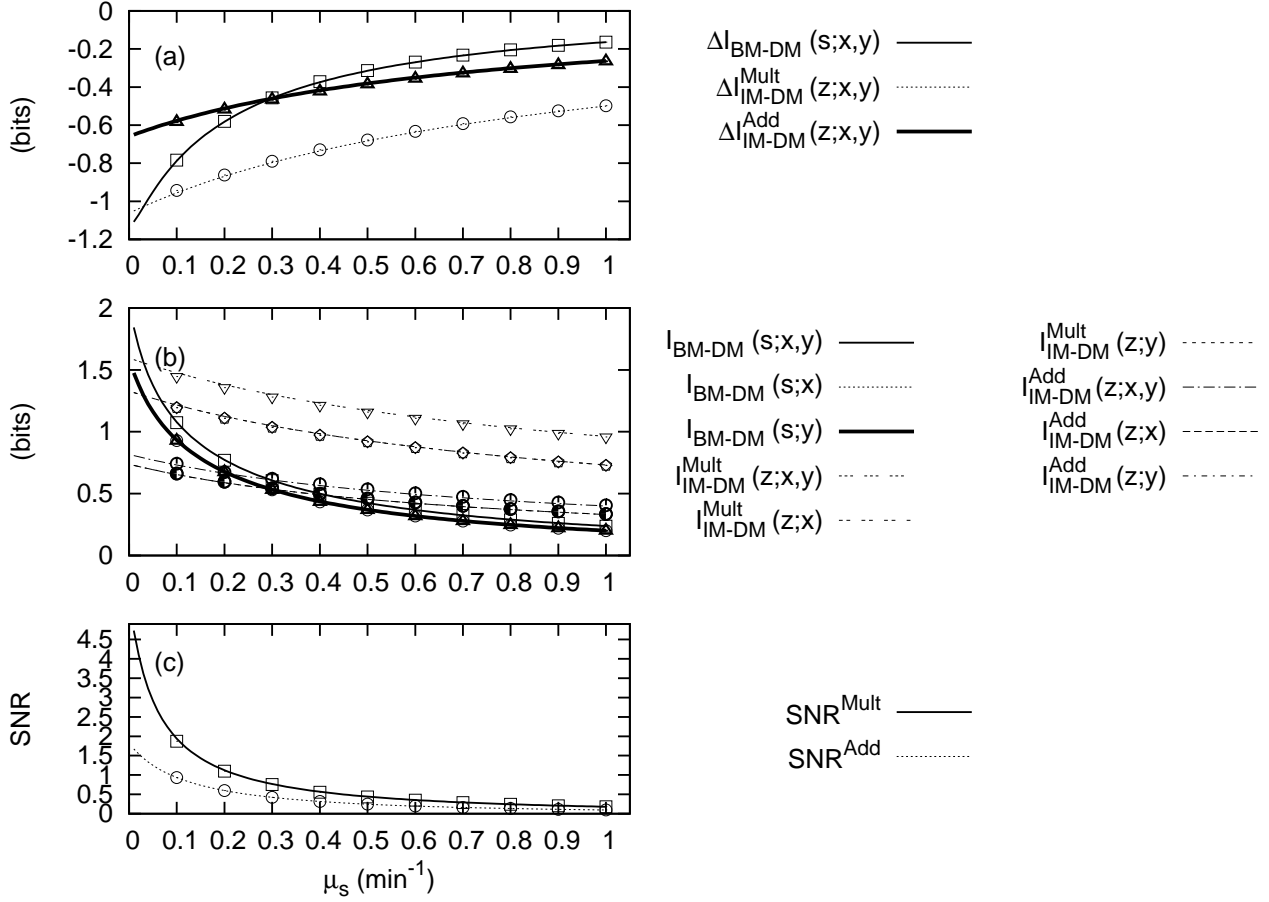


FIG. 2. (a) The net synergy for BM-DM ( $\Delta I_{BM-DM}(s;x,y)$ ), IM-DM ( $\Delta I_{IM-DM}^{Mult}(z;x,y)$  and  $\Delta I_{IM-DM}^{Add}(z;x,y)$ ), (b) Different three variable and two variable MI for BM-DM and IM-DM, (c)  $SNR^{Mult}$  and  $SNR^{Add}$  as functions of  $\mu_s$ . The lines are due to analytical results and the symbols represent numerical data generated using Gillespie's algorithm<sup>77,78</sup> with an ensemble averaging over  $10^6$  independent time series. The constraint relations for species populations are  $\langle s \rangle = 10$ ,  $\langle x \rangle = 100$ ,  $\langle y \rangle = 100$  and,  $\langle z \rangle = 100$  all in molecules/ $V$  with  $V$  being the unit effective cellular volume. The rate parameters relevant for BM-DM and IM-DM are  $k_s = \mu_s \langle s \rangle$ ,  $k_x = \mu_x \langle x \rangle ((K_1^n + \langle s \rangle^n) / \langle s \rangle^n)$ ,  $k_y = \mu_y \langle y \rangle ((K_2^n + \langle s \rangle^n) / \langle s \rangle^n)$ ,  $k_z = \mu_z \langle z \rangle (\frac{\langle x \rangle^n}{K_3^n + \langle x \rangle^n} + \frac{\langle y \rangle^n}{K_4^n + \langle y \rangle^n})^{-1}$  and,  $k'_z = \mu_z \langle z \rangle ((K_3^n + \langle x \rangle^n) / \langle x \rangle^n) ((K_4^n + \langle y \rangle^n) / \langle y \rangle^n)$ .  $K_1 = K_2 = 90$ ,  $K_3 = K_4 = 100$  all in molecules/ $V$  with  $V$  being the unit effective cellular volume,  $\mu_x = \mu_y = 0.5$  min<sup>-1</sup>,  $\mu_z = 5$  min<sup>-1</sup>. In both the cases, we have used  $n = 1$ .

appearing in the denominators of the MI-s present in Eqs. (10,11) are the corresponding conditional variances and can be computed as follows<sup>37</sup>

$$\Sigma(s|x) =: \Sigma(s) - \Sigma(s,x)[\Sigma(x)]^{-1}\Sigma(x,s), \quad (12)$$

$$\Sigma(s|y) =: \Sigma(s) - \Sigma(s,y)[\Sigma(y)]^{-1}\Sigma(y,s), \quad (13)$$

$$\begin{aligned} \Sigma(s|x,y) =: & \Sigma(s) - \begin{pmatrix} \Sigma(s,x) & \Sigma(s,y) \end{pmatrix} \\ & \times \begin{pmatrix} \Sigma(x) & \Sigma(x,y) \\ \Sigma(y,x) & \Sigma(y) \end{pmatrix}^{-1} \begin{pmatrix} \Sigma(x,s) \\ \Sigma(y,s) \end{pmatrix}. \end{aligned} \quad (14)$$

We note that the covariances are symmetric, e.g.  $\Sigma(s,x) = \Sigma(x,s)$  etc. Similarly, one can compute necessary expressions involving  $x$ ,  $y$  and,  $z$ . For explicit generalized forms of the variance and covariance, we refer to the Appendix.

### III. RESULTS AND DISCUSSION

In this section, we explore the parametric dependence of information transmission in terms of the net synergy in the DM. To this end, we have identified two sub-motifs namely the BM-DM and the IM-DM, embedded within the DM (see Fig. 1). The net synergy is explored in the independent BM and IM (see Fig. 1) and also when both the motifs are ingrained in the DM as sub-motifs. This has been done with an aim to quantify the dependence of DM on two of its sub-motifs in the context of information processing and mitigation of noise. In both the analytical and numerical calculations, we keep the species population fixed at steady state e.g.,  $\langle s \rangle = 10$ ,  $\langle x \rangle = 100$ ,  $\langle y \rangle = 100$  and,  $\langle z \rangle = 100$ , irrespective of the network architecture examined. We note here that the unit of the population we use is molecules/ $V$ , where  $V$  is unit effective cellular volume. The steady state population level we use, are experimentally observed in transcription control network<sup>69,74,83</sup>. The strategy of copy number constancy has the advantage of comparing the optimal performances of species at steady state<sup>32</sup>. The constraint of population constancy governs choices of the synthesis rate parameters while one can make independent choices for the degradation rate parameters.

#### A. Variation in the time scale of input signal shows effective redundancy empowers signal fidelity

Fig. 2 shows the net synergy  $\Delta I_{BM-DM}(s; x, y)$  and  $\Delta I_{IM-DM}(z; x, y)$  for BM-DM and IM-DM, respectively, along with corresponding two-variable and three-variable MI and the SNR as a function of  $\mu_s$  for  $\mu_x = \mu_y = 0.5 \text{ min}^{-1}$  and  $\mu_z = 5 \text{ min}^{-1}$ .  $\Delta I_{IM-DM}(z; x, y)$ , MI-s and, SNR-s are theoretically calculated for additive and multiplicative integration and denoted by  $\Delta I_{IM-DM}^{Add}$ ,  $\Delta I_{IM-DM}^{Mult}$ ,  $I^{Add}(z; x, y)$  and  $I^{Mult}(z; x, y)$  etc.,  $\text{SNR}^{Add}$  and,  $\text{SNR}^{Mult}$ , respectively. To check the validity of our analytical calculations, we also execute numerical simulation using stochastic simulation algorithm<sup>77,78</sup>. Table I provides the detailed information on the reaction channels implemented in stochastic simulation. For example, in the BM  $k_s = \mu_s \langle s \rangle$ ,  $k_x = \mu_x \langle x \rangle ((K_1^n + \langle s \rangle^n) / \langle s \rangle^n)$  and,  $k_y = \mu_y \langle y \rangle ((K_2^n + \langle s \rangle^n) / \langle s \rangle^n)$ . Similarly for the IM we use,  $k_x = \mu_x \langle x \rangle$ ,  $k_y = \mu_y \langle y \rangle$ ,  $k_z = \mu_z \langle z \rangle (\frac{\langle x \rangle^n}{K_3^n + \langle x \rangle^n} + \frac{\langle y \rangle^n}{K_4^n + \langle y \rangle^n})^{-1}$  and,  $k'_z = \mu_z \langle z \rangle ((K_3^n + \langle x \rangle^n) / \langle x \rangle^n) ((K_4^n + \langle y \rangle^n) / \langle y \rangle^n)$ . Finally for the DM the synthesis rate parameters are as follows:  $k_s = \mu_s \langle s \rangle$ ,  $k_x = \mu_x \langle x \rangle ((K_1^n + \langle s \rangle^n) / \langle s \rangle^n)$ ,  $k_y = \mu_y \langle y \rangle ((K_2^n + \langle s \rangle^n) / \langle s \rangle^n)$ ,  $k_z = \mu_z \langle z \rangle (\frac{\langle x \rangle^n}{K_3^n + \langle x \rangle^n} + \frac{\langle y \rangle^n}{K_4^n + \langle y \rangle^n})^{-1}$  and,  $k'_z = \mu_z \langle z \rangle ((K_3^n + \langle x \rangle^n) / \langle x \rangle^n) ((K_4^n + \langle y \rangle^n) / \langle y \rangle^n)$ . We note that while generating the analytical and numerical results in Fig. 2, we have used  $n = 1$  as  $n > 1$  brings in higher order nonlinearity that may cause breakdown of LNA.

The net synergy profiles are constrained in the negative domain and show a hyperbolic trend, as a function of  $\mu_s$ . As  $\mu_s$  increases, the negative domain gradually shrinks since synergy overpowers redundancy due to  $\Delta I = I_S - I_R$ . In other words, the effective redundancy  $I_{ER}$  decreases and gradually makes way for information independence. As conceptualised within the framework of PID, one can conveniently assume that redundancy takes care of common information sharing among the nodes of the diamond motif. Some of the key observations from the net synergy profiles shown in Fig. 2a, are as follows: For low  $\mu_s$ ,

$$\Delta I_{IM-DM}^{Add} > \Delta I_{BM-DM} > \Delta I_{IM-DM}^{Mult}.$$

Similarly, for high  $\mu_s$ ,

$$\Delta I_{BM-DM} > \Delta I_{IM-DM}^{Add} > \Delta I_{IM-DM}^{Mult}.$$

These trends can be justified as one takes into account the corresponding MI profiles shown in Fig. 2b where the following ordering exists,

$$\begin{aligned} I_{IM-DM}^{Mult}(z; x, y) &> I_{IM-DM}^{Mult}(z; x) = I_{IM-DM}^{Mult}(z; y) > \\ I_{IM-DM}^{Add}(z; x, y) &> I_{IM-DM}^{Add}(z; x) = I_{IM-DM}^{Add}(z; y). \end{aligned}$$

In addition, one should also take note of the following inequality in the MI differences,

$$I_{IM-DM}^{Mult}(z; x, y) - I_{IM-DM}^{Mult}(z; x) > I_{IM-DM}^{Add}(z; x, y) - I_{IM-DM}^{Add}(z; x).$$

Along with  $I_{IM-DM}^{Mult}(z; y)$  and  $I_{IM-DM}^{Add}(z; y)$ , these differences ultimately guide the net synergy. Furthermore, for low  $\mu_s$ ,

$$\begin{aligned} I_{BM-DM}(s; x, y) &> I_{BM-DM}(s; x) = I_{BM-DM}(s; y) > \\ I_{IM-DM}^{Add}(z; x, y) &> I_{IM-DM}^{Add}(z; x) = I_{IM-DM}^{Add}(z; y). \end{aligned}$$



TABLE I. Table of the chemical reactions and associated propensities for the diamond motif. Here, S, X, Y and, Z stand for biochemical species and  $s, x, y$  and,  $z$  represent copy numbers of the respective species expressed in molecules/ $V$  with  $V$  being the unit effective cellular volume. For X and Y mediated production of Z, an additive and a multiplicative logic is used. It results in two different synthesis rates, i.e.  $k_z$  and  $k'_z$ , respectively. We have taken Hill coefficient  $n = 1$ . The rate constants are expressed in  $\text{min}^{-1}$ .

Biochemical Processes	Reaction	Propensity
Synthesis of S	$\phi \rightarrow S$	$k_s$
Degradation of S	$S \rightarrow \phi$	$\mu_s s$
S mediated synthesis of X	$S \rightarrow S + X$	$k_x \frac{s^n}{K_1^n + s^n}$
Degradation of X	$X \rightarrow \phi$	$\mu_x x$
S mediated synthesis of Y	$S \rightarrow S + Y$	$k_y \frac{s^n}{K_2^n + s^n}$
Degradation of Y	$Y \rightarrow \phi$	$\mu_y y$
X, Y mediated synthesis of Z (Additive)	$X+Y \rightarrow X+Y+Z$	$k_z \left( \frac{x^n}{K_3^n + x^n} + \frac{y^n}{K_4^n + y^n} \right)$
X, Y mediated synthesis of Z (Multiplicative)	$X+Y \rightarrow X+Y+Z$	$k'_z \frac{x^n}{K_3^n + x^n} \frac{y^n}{K_4^n + y^n}$
Degradation of Z	$Z \rightarrow \phi$	$\mu_z z$

On a similar note, for high  $\mu_s$ ,

$$I_{IM-DM}^{Add}(z; x, y) > I_{IM-DM}^{Add}(z; x) = I_{IM-DM}^{Add}(z; y) > I_{BM-DM}(s; x, y) > I_{BM-DM}(s; x) = I_{BM-DM}(s; y).$$

We also note that  $I_{BM-DM}(s; x, y) - I_{BM-DM}(s; x)$  decreases rapidly in comparison with  $I_{IM-DM}^{Add}(z; x, y) - I_{IM-DM}^{Add}(z; x)$ , whereas the MI profiles of BM-DM also decrease rapidly compared to MI profiles for additive and multiplicative IM-DM (see Fig. 2b). This contrast in slowing down gets reflected in the net synergy. It is observed that  $\Delta I_{BM-DM}$  occupies a long range and gets nearer to zero value in comparison with both  $\Delta I_{IM-DM}^{Add}$  and  $\Delta I_{IM-DM}^{Mult}$ .

We also performed a parallel investigation on SNR, defined as  $\Sigma^2(s, z)/[\Sigma(s)\Sigma(z) - \Sigma^2(s, z)]^{26}$ . SNR is calculated taking S as the signal and Z as the response of the DM. Both  $\text{SNR}^{Add}$  and  $\text{SNR}^{Mult}$  shows opposite trend with respect to  $\Delta I_{IM-DM}^{Add}$  and  $\Delta I_{IM-DM}^{Mult}$ , respectively. We note that  $\text{SNR}^{Mult} > \text{SNR}^{Add}$  and shows opposite trend of  $\Delta I_{IM-DM}^{Add} > \Delta I_{IM-DM}^{Mult}$ . These trends are suggestive of the fact that with enhanced effective redundancy  $I_{ER}$ , the fidelity of the signaling pathway also gets strengthened. A similar observation was previously reported for a two-step cascade motif<sup>53</sup>. The observed agreement between the analytical and numerical results are indicative of the effectiveness of LNA applied in our calculation.

Here, we want to draw attention to the apparent similarities between net synergy based results from two different motifs namely TSC as in Ref. 53 and, for DM in the present manuscript. Both systems show an ample amount of effective redundancy  $I_{ER}$  and also the signal fidelity increases with it. It should be noted that DM is constituted from TSC by duplicating its middle node and associated edges. For our current purpose, we carved out BM and IM from DM. It is important to point out that effective redundancy  $I_{ER}$  gets manifested in TSC and DM using visibly different inter-relationship of the associated two-variable and three-variable MI-s. For a TSC motif  $S \rightarrow X \rightarrow Y$ , we got  $I(s; x, y) \approx I(s; x) > I(s; y)$  both for the linear and nonlinear form of inter-species interactions<sup>53</sup>. Therefore, the net synergy picks up its major share from  $I(s; y)$ , i.e.  $\Delta I(s; x, y) \approx -I(s; y)$ . However, this is not the case in BM (equivalent to BM-DM) and, IM-DM (see Fig. 2(a-b) and Fig. 5(b) with Eq. (7-8)). In these architectures, none of the individual three-variable and two-variable MI terms cancels each other as in TSC case. All of these terms contribute to generate the net synergy profiles. This trend also holds for IM which produces effective synergy  $I_{ES}$  (see Fig. 5(a) with Eq. (8)). As an extra piece of observation related to this DM-centric study, we know that effective redundancy  $I_{ER}$  empowers signal fidelity with respect to both additive and multiplicative signal integration mechanism. A TSC motif due to its linear architecture, can not provide this specific insight. Hence, the creation of effective redundancy  $I_{ER}$  is mechanistically different in a TSC motif and BM (BM-DM) and, IM-DM.

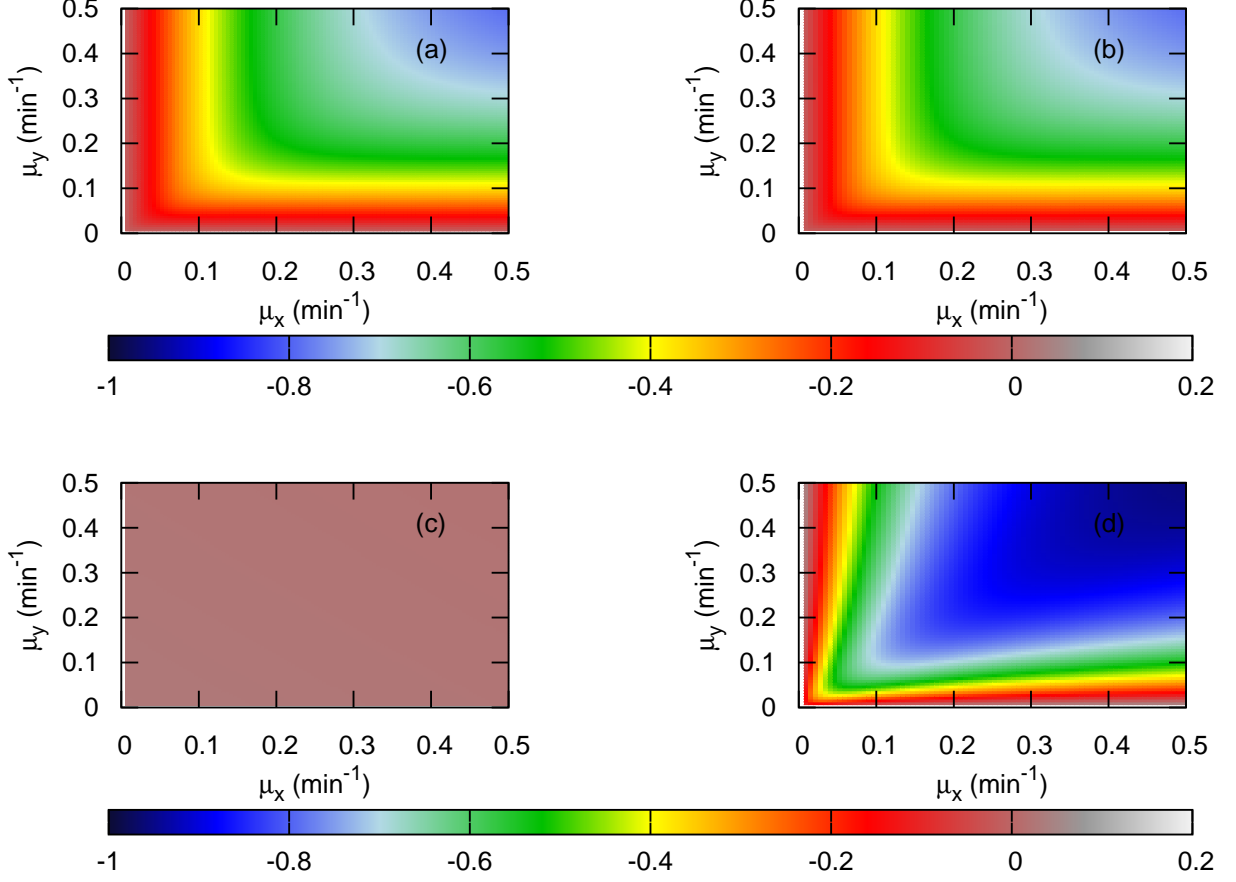


FIG. 3. Theoretical profiles (a)-(b) show variations in  $\Delta I_{BM}(s; x, y)$  and  $\Delta I_{BM-DM}(s; x, y)$  measured in bits as functions of  $\mu_x$  and  $\mu_y$ , respectively. Similarly, (c)-(d) show variations in  $\Delta I_{IM}^{Mult}(z; x, y)$  and  $\Delta I_{IM-DM}^{Mult}(z; x, y)$  measured in bits as functions of  $\mu_x$  and  $\mu_y$ , respectively. These maps are generated keeping  $\mu_s = 0.1 \text{ min}^{-1}$  and  $\mu_z = 5 \text{ min}^{-1}$ . The synthesis rate parameters for BM are  $k_s = \mu_s \langle s \rangle$ ,  $k_x = \mu_x \langle x \rangle ((K_1^n + \langle s \rangle^n) / \langle s \rangle^n)$  and,  $k_y = \mu_y \langle y \rangle ((K_2^n + \langle s \rangle^n) / \langle s \rangle^n)$ . For IM the synthesis rates are  $k_x = \mu_x \langle x \rangle$ ,  $k_y = \mu_y \langle y \rangle$  and,  $k'_z = \mu_z \langle z \rangle ((K_3^n + \langle x \rangle^n) / \langle x \rangle^n) ((K_4^n + \langle y \rangle^n) / \langle y \rangle^n)$ . The synthesis rate parameters associated with DM are  $k_s = \mu_s \langle s \rangle$ ,  $k_x = \mu_x \langle x \rangle ((K_1^n + \langle s \rangle^n) / \langle s \rangle^n)$ ,  $k_y = \mu_y \langle y \rangle ((K_2^n + \langle s \rangle^n) / \langle s \rangle^n)$  and,  $k'_z = \mu_z \langle z \rangle ((K_3^n + \langle x \rangle^n) / \langle x \rangle^n) ((K_4^n + \langle y \rangle^n) / \langle y \rangle^n)$ . We maintain  $\langle s \rangle = 10$ ,  $\langle x \rangle = 100$ ,  $\langle y \rangle = 100$ ,  $\langle z \rangle = 100$ ,  $K_1 = K_2 = 90$ ,  $K_3 = K_4 = 100$  all in molecules/ $V$  with  $V$  being the unit effective cellular volume and,  $n = 1$ .

## B. Common source of input fluctuations generates effective redundancy

The two maps in Fig. 3(a,b) are generated by scanning the parameter spaces of  $\mu_x$  and  $\mu_y$  for fixed signal relaxation rate  $\mu_s = 0.1 \text{ min}^{-1}$  and depict the net synergy  $\Delta I_{BM}(s; x, y)$  and  $\Delta I_{BM-DM}(s; x, y)$  of BM and BM-DM, respectively. Fig. 4(a,b) do the same for  $\mu_s = 1 \text{ min}^{-1}$ . The maps of the net synergy  $\Delta I_{IM}^{Mult}(z; x, y)$  and  $\Delta I_{IM-DM}^{Mult}(z; x, y)$  of IM and IM-DM, respectively, are also shown in Fig. 3(c,d) and Fig. 4(c,d) for  $\mu_s = 0.1 \text{ min}^{-1}$  and  $\mu_s = 1 \text{ min}^{-1}$ , respectively. Fig. 3(c) shows positive net synergy  $\Delta I_{IM}^{Mult}(z; x, y)$  or effective synergy  $I_{ES}$  spanning the entire parameter range. On the other hand, Fig. 3(d) shows redundancy is empowered in comparison with synergy in most of the area of the net synergy profile  $\Delta I_{IM-DM}^{Mult}(z; x, y)$  consisting of a larger negative domain along with a minuscule positive valued region. In short, moving from Fig. 3(c) to Fig. 3(d), effective redundancy  $I_{ER}$  takes up control over effective synergy  $I_{ES}$ . In comparison with their corresponding counterparts in Fig. 3, Fig. 4(a,d) shows the interplay between synergy and redundancy to be less favorable to redundant information. This is reflected in the shrunken range of variation of the net synergy.

To comprehend the nature of the net synergy profiles, we take note of the fact that there are multiple time scales involved with the biochemical species constituting different topologies (BM, BM-DM, IM, IM-DM and, DM). These time scales play crucial roles to affect the information flow along the motif. They sometimes facilitate propagation of

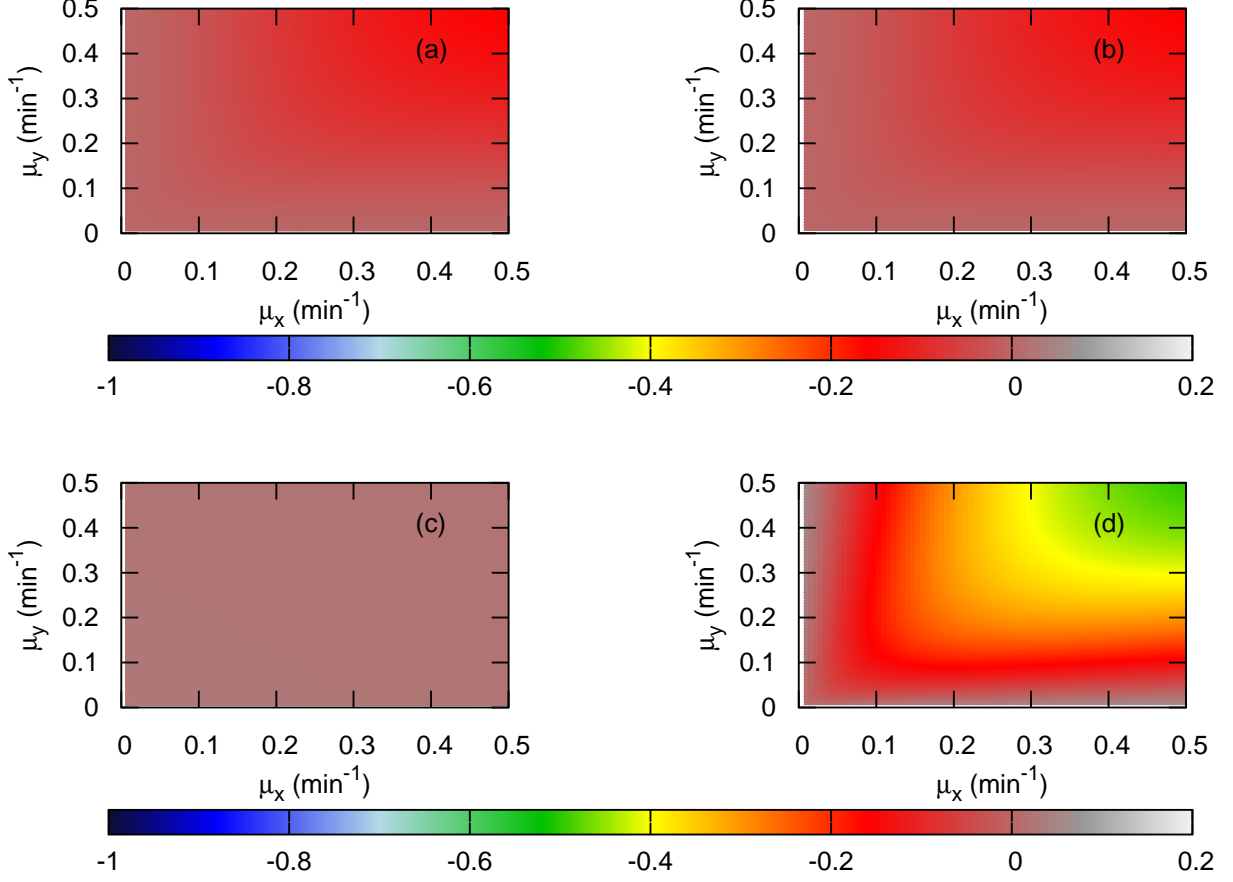


FIG. 4. Theoretical profiles (a)-(b) show variations in  $\Delta I_{BM}(s; x, y)$  and  $\Delta I_{BM-DM}(s; x, y)$  measured in bits as functions of  $\mu_x$  and  $\mu_y$ , respectively. Similarly, (c)-(d) show variations in  $\Delta I_{IM}^{Mult}(z; x, y)$  and  $\Delta I_{IM-DM}^{Mult}(z; x, y)$  measured in bits as functions of  $\mu_x$  and  $\mu_y$ , respectively. These maps are generated keeping  $\mu_s = 1 \text{ min}^{-1}$  and  $\mu_z = 5 \text{ min}^{-1}$ . The synthesis rate parameters for BM are as follows:  $k_s = \mu_s \langle s \rangle$ ,  $k_x = \mu_x \langle x \rangle ((K_1^n + \langle s \rangle^n) / \langle s \rangle^n)$  and,  $k_y = \mu_y \langle y \rangle ((K_2^n + \langle s \rangle^n) / \langle s \rangle^n)$ . For IM these are  $k_x = \mu_x \langle x \rangle$ ,  $k_y = \mu_y \langle y \rangle$  and,  $k'_z = \mu_z \langle z \rangle ((K_3^n + \langle x \rangle^n) / \langle x \rangle^n) ((K_4^n + \langle y \rangle^n) / \langle y \rangle^n)$ . The corresponding set for DM is as follows:  $k_s = \mu_s \langle s \rangle$ ,  $k_x = \mu_x \langle x \rangle ((K_1^n + \langle s \rangle^n) / \langle s \rangle^n)$ ,  $k_y = \mu_y \langle y \rangle ((K_2^n + \langle s \rangle^n) / \langle s \rangle^n)$  and,  $k'_z = \mu_z \langle z \rangle ((K_3^n + \langle x \rangle^n) / \langle x \rangle^n) ((K_4^n + \langle y \rangle^n) / \langle y \rangle^n)$ . We maintain  $\langle s \rangle = 10$ ,  $\langle x \rangle = 100$ ,  $\langle y \rangle = 100$ ,  $\langle z \rangle = 100$ ,  $K_1 = K_2 = 90$ ,  $K_3 = K_4 = 100$  all in molecules/ $V$  with  $V$  being the unit effective cellular volume and,  $n = 1$ .

information and hinder otherwise<sup>34,57-59</sup>. Now, we re-express the preceding statement as a guiding principle to analyze information flow in the motif under investigation. Whenever the upstream species concentration fluctuates slowly as compared to its immediate downstream species (i.e. the upstream species has got a relatively small relaxation rate with respect to that of the downstream species) it helps the downstream species to sense the upstream fluctuations accurately thereby allowing information flow to occur. In the opposite scenario, the downstream species fails to follow the rapid upstream fluctuations with adequate precision thereby obstructing the information propagation. In both the cases mentioned, the corresponding effects get pronounced depending upon the extent of separation of these time scales with respect to each other<sup>59</sup>. The idea of separation of time scales seems very useful to rationalize this low-pass filter like characteristics of DM. Surprisingly, this simple physical analog sets up the logical framework which encapsulates the phenomenon of frequency dependent encoding, processing and, decoding mechanisms of biological signals<sup>28</sup>.

The net synergy profiles in Fig. 2(a) can be well understood keeping the above-mentioned principle in perspective. The range of variation of  $\mu_s$  spans regions with  $\mu_s < \mu_x(\mu_y)$ ,  $\mu_s = \mu_x(\mu_y)$  and  $\mu_s > \mu_x(\mu_y)$ . At the same time, by keeping  $\mu_z = 5 \text{ min}^{-1}$  which is 10 times faster than  $\mu_x(\mu_y)$ , fixed at  $0.5 \text{ min}^{-1}$ ; adequate amount of information flow is allowed for convenience. It is clear from Fig. 2(a) that as the source species fluctuates faster compared to downstream species, transmitted amount of effective redundancy  $I_{ER}$  decreases.

In Fig. 3(a), as we move along the diagonal from low  $\mu_x(\mu_y)$  to high  $\mu_x(\mu_y)$ , it is observed that the value of net synergy  $\Delta I_{BM}(s; x, y)$  becomes more negative implying increase in effective redundancy  $I_{ER}$ . Negative  $\Delta I$  means  $I_R > I_S$  and increment in negativity may be caused either keeping  $I_S$  fixed and increasing  $I_R$  or changing both  $I_S$  and  $I_R$  while maintaining the rate of change of  $I_R >$  the rate of change of  $I_S$ . In this sense, we infer that  $I_{ER}$  rises. It should be noted that moving along this diagonal direction, both the downstream species X and Y become more sensitive towards the signal (S) fluctuations thereby get to harness more information. By this token, according to the definitions of  $\Delta I$  prescribed by PID, the amount of common or redundant information content between X and Y about S increases causing the net synergy to decrease.

One can compare the net synergy profiles of BM in Figs. 3(a) and 4(a) subject to variation in the signal relaxation. It is visible that with increased  $\mu_s$  from  $0.1 \text{ min}^{-1}$  to  $1 \text{ min}^{-1}$ , the domain of net synergy shifts close to zero value. Such a change in the nature of the net synergy profile is due to the fact that in Fig. 4(a) fixing  $\mu_s = 1 \text{ min}^{-1}$  blocks information flow significantly in the motif since both the downstream species X and Y fluctuates in the range of  $0 - 0.5 \text{ min}^{-1}$ , slower than the time scale of fluctuations of the source species S.

In Fig. 3(c), the net synergy  $\Delta I_{IM}^{Mult}(z; x, y)$  is entirely constrained in the positive domain, i.e. we get effective synergy  $I_{ES}$ . Since we have not specified synergy and redundancy independently in a quantitative manner, we are not certain that whether this positive nature is due to pure synergy or synergy being dominant over redundancy, but we can at least make an intuitive inference. It has a certain benefit not to opt for any specific definition of any of the PID terms, thereby keeping ample generality in the treatment of the motif which may be subjected to some hitherto unknown biological constraints. Hence, any concrete comment on the extent of both synergy and redundancy can be made only in a comparative manner using a relative scaling. Redundancy being sharing of information<sup>37</sup>, may originate from a common source which in this case (i.e. IM) is absent. There are two uncorrelated source X and Y and single target Z in IM unlike in BM where the targets X and Y share a common source S. We conjecture here that the absence of a common source is suggestive of pure synergy over the entire parameter space (Figs. 3(c) and 4(c)). At par with same line of argument, it can be stated that, effective redundancy  $I_{ER}$  arises in TSC motif ( $S \rightarrow X \rightarrow Y$ ), because information source variable S is common for the information target variables X and Y while computing the net synergy  $\Delta I(s; x, y)$  in Ref 53. In the dynamical sense also, the effect of signaling source S is stochastically manifested in X first and finally in Y via X. Therefore, the concept of commonality in input fluctuations creating effective redundancy  $I_{ER}$  remains in place. Information-theoretic analysis grounded in neurophysiological recordings in the primary visual context of anesthetized macaque monkeys has successfully applied the information breakdown methodology (IBM)<sup>84</sup>, similar to PID discussed in our current work. We invoke this particular analysis to place some intuitive aspects of redundant and synergistic information in our model system through a qualitative mapping from neuronal network to GRN. As in Ref. 84 and 85, IBM prescribes the following decomposition:

$$I_{ensemble} = I_{lin} + I_{sig\text{sim}} + I_{cor,dep} + I_{cor,ind}. \quad (15)$$

For BM and BM-DM,  $I_{ensemble}^{BM(BM-DM)}(s; x, y) \equiv I_{BM(BM-DM)}(s; x, y)$ ,  $I_{lin}^{BM(BM-DM)} \equiv I_{BM(BM-DM)}(s; x) + I_{BM(BM-DM)}(s; y)$ . Here, we denote both  $I_{ensemble}^{BM(BM-DM)}(s; x, y)$  and  $I_{lin}^{BM(BM-DM)}(s; x, y)$  by a single notation  $I_{ensemble}^{BM(BM-DM)}(s; x, y)$  and we use this type of notation for the rest of the information terms considering every motifs and sub-motifs. Therefore,  $I_{ensemble}^{BM(BM-DM)}(s; x, y) - I_{lin}^{BM(BM-DM)}(s; x, y) = I_{BM(BM-DM)}(s; x, y) - I_{BM(BM-DM)}(s; x) - I_{BM(BM-DM)}(s; y)$ . According to PID, the expression on the right-hand side of the last expression is defined as the net synergy,  $\Delta I = I_S - I_R$  (see Eq. 9). Taking the lead from Ref 84, we put  $I_{sig\text{sim}}^{BM(BM-DM)}(s; x, y)$  into perspective of GRN. This signal similarity measure accounts for the reduction in  $I_{ensemble}^{BM(BM-DM)}(s; x, y)$  caused by the similar type of activation mechanisms represented by the parameters associated with the edges, e.g.  $S \rightarrow X$  and  $S \rightarrow Y$  in BM and BM-DM. The corresponding production terms (See Table I) are similar as  $K_1 = K_2$ ,  $k_x = k_y$  (given  $\langle x \rangle = \langle y \rangle$  and  $\mu_x = \mu_y$ ) and  $n = 1$  for both species X and Y. Thus, this component contributes negatively for BM and, BM-DM.  $I_{cor,dep}$  and  $I_{cor,ind}$  designates signal-dependent correlation induced information and signal-independent correlation induced information, respectively for all motifs and sub-motifs. By information-theoretic definition,  $I_{cor,dep} \geq 0$  in general. Since in our model system, all the correlation functions are non-negative, and noise profiles are uncorrelated (see section II for the noise characteristics),  $I_{cor,ind}$  should be zero for all the motifs and sub-motifs. In the case of BM and BM-DM, if we take into consideration the presence of a common source of fluctuations (S), we can justify the predominantly negative trend in their net synergy profiles by utilizing the negative contribution of  $I_{sig\text{sim}}^{BM(BM-DM)}(s; x, y)$ . Considering these points, we re-write Eq. 15 for BM and BM-DM as follows:

$$\Delta I_{BM(BM-DM)}(s; x, y) = |I_{cor,dep}^{BM(BM-DM)}(s; x, y)| - |I_{sig\text{sim}}^{BM(BM-DM)}(s; x, y)|. \quad (16)$$

Where  $|\dots|$  designate the magnitude of corresponding information component. For IM and IM-DM,  $I_{ensemble}^{IM(IM-DM)}(z; x, y) \equiv$

$I_{IM(IM-DM)}(z; x, y)$ ,  $I_{lin}^{IM(IM-DM)} \equiv I_{IM(IM-DM)}(z; x) + I_{IM(IM-DM)}(z; y)$ . Therefore,  $I_{ensemble}^{IM(IM-DM)} - I_{lin}^{IM(IM-DM)} = I_{IM(IM-DM)}(z; x, y) - I_{IM(IM-DM)}(z; x) - I_{IM(IM-DM)}(z; y)$ . These expressions are valid for both additive and multiplicative signal integration mechanisms. We will further denote additive and multiplicative integration scheme by writing ‘-Add’, ‘-Mult’ respectively. Now, for the edges  $X \rightarrow Z$  and  $Y \rightarrow Z$  in IM-Add, IM-Mult, IM-DM-Add and, IM-DM-Mult, we have architectural similarity maintained by similar production functions with a single  $k_z$ ,  $k'_z$ ,  $K_3 = K_4$ ,  $k_x = k_y$  (given  $\langle x \rangle = \langle y \rangle$  and  $\mu_x = \mu_y$ ) and  $n = 1$ . However, surprisingly for IM-Add and IM-Mult, even with  $\Sigma(x, y) = 0$  (implying  $I_{cor,dep}^{IM-Add}(z; x, y) = I_{cor,dep}^{IM-Mult}(z; x, y) = 0$ ), we have  $\Delta I_{IM-Add(IM-Mult)}(z; x, y) > 0$ . To rationalize this observation, we note that since in IM-Add and IM-Mult, there is no common source of fluctuations present but the system still possesses similar signaling branches,  $I_{sigstim}$  contributes positively as follows:

$$\Delta I_{IM-Add(IM-Mult)}(z; x, y) = |I_{sigstim}^{IM-Add(IM-Mult)}(z; x, y)|. \quad (17)$$

In IM-DM-Add and IM-DM-Mult, due to the presence of common input S and similarities in between two bifurcating branch ( $S \rightarrow X$  and  $S \rightarrow Y$ ) and similarities in between two integrating branch ( $X \rightarrow Z$  and  $Y \rightarrow Z$ )  $I_{sigstim}^{IM-DM-Add}(z; x, y)$  and  $I_{sigstim}^{IM-DM-Mult}(z; x, y)$  is negative as in BM and BM-DM. And by and large it overpowers  $I_{cor,dep}^{IM-DM-Add}(z; x, y)$  and  $I_{cor,dep}^{IM-DM-Mult}(z; x, y)$  respectively to make  $\Delta I_{IM-DM-Add}(z; x, y) < 0$  and  $\Delta I_{IM-DM-Mult}(z; x, y) < 0$  respectively according to the following two consecutive expressions:

$$\Delta I_{IM-DM-Add}(z; x, y) = |I_{cor,dep}^{IM-DM-Add}(z; x, y)| - |I_{sigstim}^{IM-DM-Add}(z; x, y)|. \quad (18)$$

$$\Delta I_{IM-DM-Mult}(z; x, y) = |I_{cor,dep}^{IM-DM-Mult}(z; x, y)| - |I_{sigstim}^{IM-DM-Mult}(z; x, y)|. \quad (19)$$

This rudimentary connection between PID and IBM is far from complete in the present model GRN systems and at best offers some speculative remarks.

In Figs. 3(d) and 4(d), the net synergy decreases along the diagonal from low  $\mu_x(\mu_y)$  to high  $\mu_x(\mu_y)$  which is at par with the previously placed argument based on the idea of separation of time scales. In Ref. 37, a dynamical system analog of IM was showcased and was noted that synergy between sources about the target, is a function of the correlation between sources. Although, there is no physical link in between the sources, (cross) correlation has been invoked in their noise processes. Our treatment does not involve noise correlation and for that matter, depends on inter-species interactions to develop correlations that further dictate the net synergy. This is rather straight-forward and does not create any misunderstanding when one tries to interpret information processing based on the connectivity diagrams of the motifs. The specialized PID namely MMI PID<sup>37</sup> defines redundancy as the minimum MI provided by the sources about the target. Synergy comes from the extra information by the weaker source given the other source is known. However, in more generalized situations, the motifs can have architecturally redundant pathways, i.e. source variables may be equally strong. This is one of the key observations from our study where we set out to map architectural redundancy and informational redundancy onto each other.

For a comparative study to explore how integration mechanism distinguishes IM and IM-DM, we set out to vary  $\mu_x(= \mu_y)$  keeping  $\mu_s$  constant and we observe in Fig. 5(a-b):

$$\Delta I_{IM}^{Mult}(+) > \Delta I_{IM}^{Add}(+) > \Delta I_{IM-DM}^{Add}(-) > \Delta I_{IM-DM}^{Mult}(-).$$

By putting + or - signs we denote the associated quantities to be positive or negative valued, respectively. To probe it further, we plotted the individual MI keeping the conditions unaltered in Fig. 5(a-b) and notice the trend

$$\begin{aligned} I_{IM-DM}^{Mult}(z; x, y) &> I_{IM-DM}^{Mult}(z; x) = I_{IM-DM}^{Mult}(z; y) > \\ I_{IM-DM}^{Add}(z; x, y) &> I_{IM-DM}^{Add}(z; x) = I_{IM-DM}^{Add}(z; y) > \\ I_{IM}^{Mult}(z; x, y) &> I_{IM}^{Mult}(z; x) = I_{IM}^{Mult}(z; y) > \\ I_{IM}^{Add}(z; x, y) &> I_{IM}^{Add}(z; x) = I_{IM}^{Add}(z; y). \end{aligned}$$

### C. Activation coefficients modulate effective redundancy and explain the trade-off between binding affinities of different biochemical species

The four edges of DM are characterized by three types of parameters namely the activation coefficients ( $K_1, K_2, K_3$  and,  $K_4$ ), the synthesis rates of biochemical species ( $k_s, k_x, k_y$  and,  $k_z$ ) and the Hill coefficient ( $n$ ) of the input



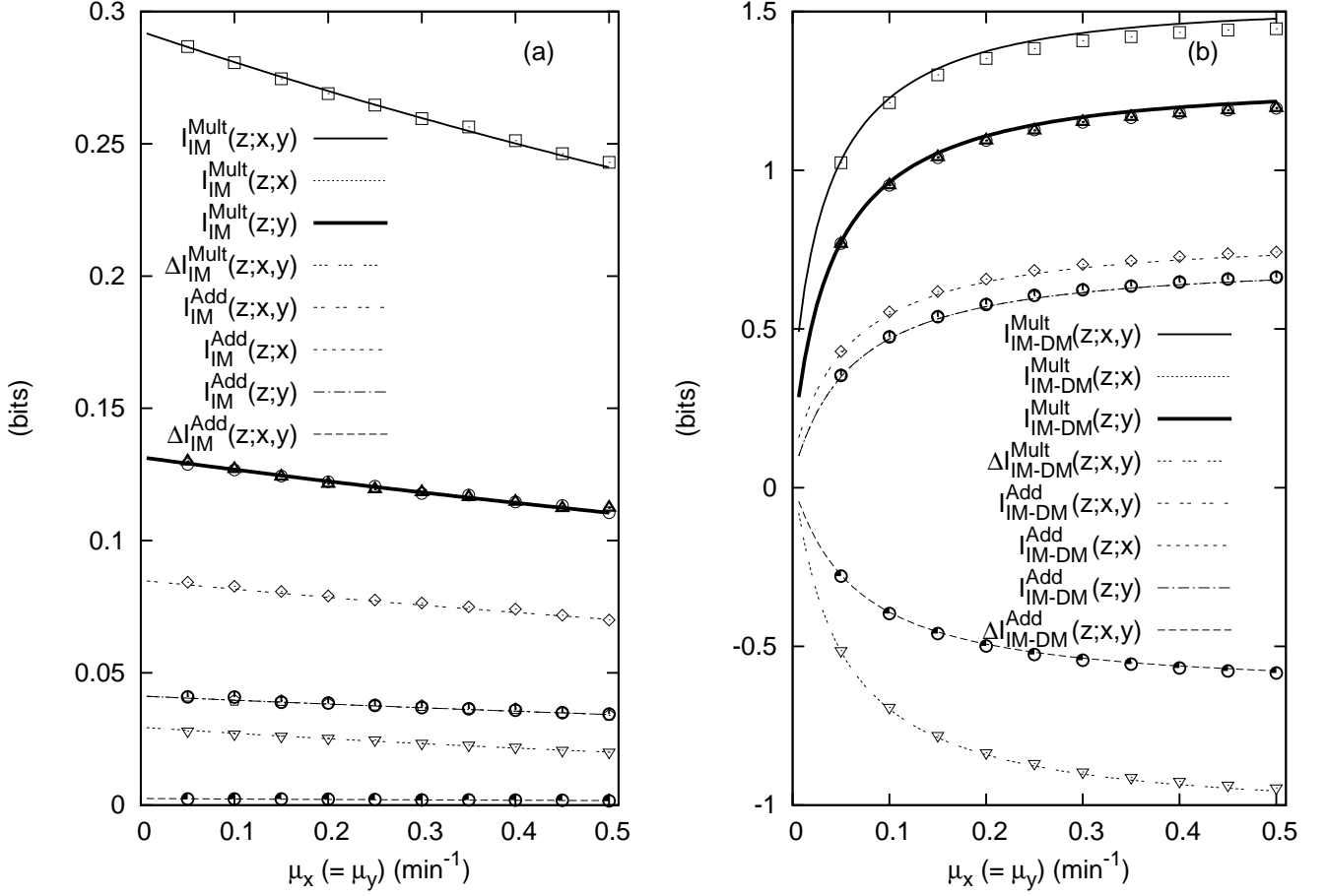


FIG. 5. Individual MI and the net synergy profiles for (a) IM and, (b) IM-DM as functions of  $\mu_x (= \mu_y)$ . The lines are due to analytical results and the symbols represent numerical data generated using Gillespie's algorithm<sup>77,78</sup> with an ensemble averaging over  $10^6$  independent time series. These profiles are generated keeping  $\mu_s = 0.1 \text{ min}^{-1}$  and  $\mu_z = 5 \text{ min}^{-1}$ . For IM the synthesis rate parameters are  $k_x = \mu_x \langle x \rangle$ ,  $k_y = \mu_y \langle y \rangle$ ,  $k_z = \mu_z \langle z \rangle \left( \frac{\langle x \rangle^n}{K_3^n + \langle x \rangle^n} + \frac{\langle y \rangle^n}{K_4^n + \langle y \rangle^n} \right)^{-1}$  and,  $k'_z = \mu_z \langle z \rangle \left( (K_3^n + \langle x \rangle^n) / \langle x \rangle^n \right) \left( (K_4^n + \langle y \rangle^n) / \langle y \rangle^n \right)$ . The corresponding set for DM is as follows:  $k_s = \mu_s \langle s \rangle$ ,  $k_x = \mu_x \langle x \rangle \left( (K_1^n + \langle s \rangle^n) / \langle s \rangle^n \right)$ ,  $k_y = \mu_y \langle y \rangle \left( (K_2^n + \langle s \rangle^n) / \langle s \rangle^n \right)$ ,  $k_z = \mu_z \langle z \rangle \left( \frac{\langle x \rangle^n}{K_3^n + \langle x \rangle^n} + \frac{\langle y \rangle^n}{K_4^n + \langle y \rangle^n} \right)^{-1}$  and,  $k'_z = \mu_z \langle z \rangle \left( (K_3^n + \langle x \rangle^n) / \langle x \rangle^n \right) \left( (K_4^n + \langle y \rangle^n) / \langle y \rangle^n \right)$ . We maintain  $\langle s \rangle = 10$ ,  $\langle x \rangle = 100$ ,  $\langle y \rangle = 100$ ,  $\langle z \rangle = 100$ ,  $K_1 = K_2 = 90$ ,  $K_3 = K_4 = 100$  all in molecules/ $V$  with  $V$  being the unit effective cellular volume and,  $n = 1$ .

regulatory functions. This minimal set of parameters ( $K_1, K_2, K_3, K_4, k_s, k_x, k_y, k_z$  and,  $n$ ) can be tuned during an experiment. It has been argued that in a continuously changing environment, these parameters associated with the population of each of the biochemical species, encounter selection pressure and thus precisely optimize the expression levels<sup>32</sup>. The time scales of their adaptability is typical of the order of hundred of generations. Experimentally,  $K_i$  ( $i = 1, 2, 3, 4$ ) can be altered by inducing mutations in the DNA sequences of the promoter region where the activator or repressor molecules bind. To alter  $k_i$  ( $i = s, x, y, z$ ), the binding site sequence for RNA polymerase are mutated. If suitable parameterization associated with a motif is done with these numbers, then experiments can be designed to place the biological motifs under selection pressure. Uri Alon points out that the resulting changes that an organism acquires under such pressure are inheritable through generations facing diverse environmental conditions<sup>32</sup>. These phenomenological inputs motivate us to link information processing with these numbers. In the previous Figs. (2-5), we have already done so by varying  $\mu_i$  ( $i = s, x, y$ ), thereby making variations in  $k_i$  ( $i = s, x, y$ ) since the constraint of fixed population size at steady state makes  $k_i \propto \mu_i$  ( $i = s, x, y, z$ ). We further reiterate that in our calculation we have used  $n = 1$  to retain the level of nonlinearity in the input regulatory functions analytically tractable under the purview of LNA.

Figure 6(a,b,c) portrays the effect of variations of  $K_1, K_2, K_3$  and,  $K_4$  on the net synergy  $\Delta I_{BM-DM}(s; x, y)$ ,

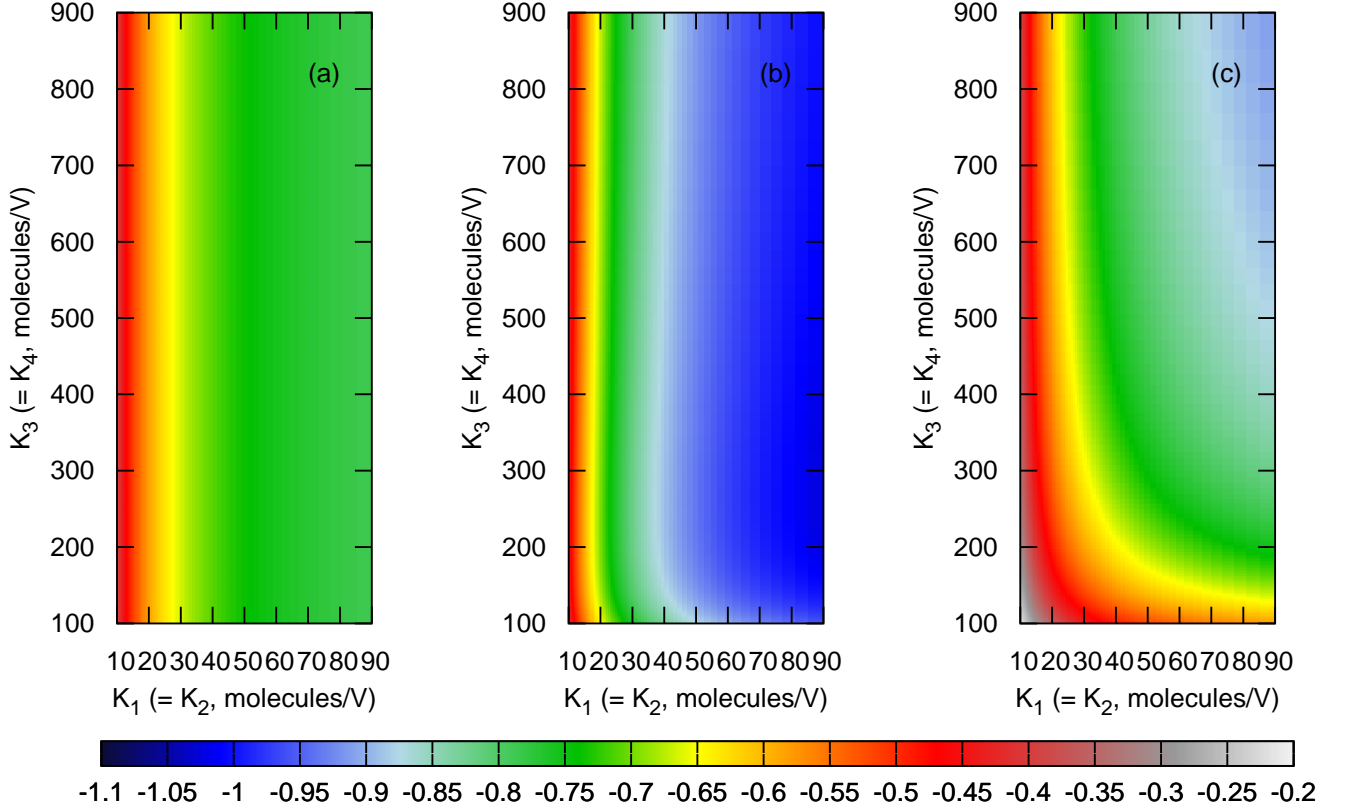


FIG. 6. The maps (a),(b) and, (c) portray  $\Delta I_{BM-DM}(s; x, y)$ ,  $\Delta I_{IM-DM}^{Mult}(z; x, y)$  and,  $\Delta I_{IM-DM}^{Add}(z; x, y)$  as functions of  $K_1(= K_2)$  and  $K_3(= K_4)$  respectively, in the unit of bits. The populations of the biochemical species S, X, Y and, Z are fixed at steady state  $\langle s \rangle = 10$ ,  $\langle x \rangle = 100$ ,  $\langle y \rangle = 100$  and,  $\langle z \rangle = 100$  all in molecules/V with  $V$  being the unit effective cellular volume. The relevant rate parameters are  $k_s = \mu_s \langle s \rangle$ ,  $k_x = \mu_x \langle x \rangle ((K_1^n + \langle s \rangle^n) / \langle s \rangle^n)$ ,  $k_y = \mu_y \langle y \rangle ((K_2^n + \langle s \rangle^n) / \langle s \rangle^n)$ ,  $k_z = \mu_z \langle z \rangle (\frac{\langle x \rangle^n}{K_3^n + \langle x \rangle^n} + \frac{\langle y \rangle^n}{K_4^n + \langle y \rangle^n})^{-1}$  and,  $k'_z = \mu_z \langle z \rangle ((K_3^n + \langle x \rangle^n) / \langle x \rangle^n) ((K_4^n + \langle y \rangle^n) / \langle y \rangle^n)$ . We use  $\mu_s = 0.1 \text{ min}^{-1}$ ,  $\mu_x = \mu_y = 0.5 \text{ min}^{-1}$ ,  $\mu_z = 5 \text{ min}^{-1}$  and,  $n = 1$  to generate the theoretical figures.

$\Delta I_{IM-DM}^{Mult}(z; x, y)$  and,  $\Delta I_{IM-DM}^{Add}(z; x, y)$ , respectively. We have kept  $\mu_s = 0.1 \text{ min}^{-1}$ ,  $\mu_x = \mu_y = 0.5 \text{ min}^{-1}$ ,  $\mu_z = 5 \text{ min}^{-1}$  to show the above-mentioned variations subject to the constraint  $K_1 = K_2$  and  $K_3 = K_4$ . By making such a set of arrangements, we have ensured adequate information flow in the motif while keeping architectural redundancy (based on interactions) in between both the bifurcating and the integrating branches. Figure 6(a) indicates that with increasing  $K_1(K_2)$ , redundancy contributes more, making the net synergy more negative. We can not rule out the presence of synergy, but it is overpowered by redundancy resulting in the production of effective redundancy  $I_{ER}$ . Similarly in Fig. 6(b), we show that with high  $K_1(K_2)$  and low  $K_3(K_4)$ , the two integrating branches of the diamond motif, contribute the maximum level of redundancy in the entire map with  $\Delta I_{IM-DM}^{Mult}(z; x, y)$  giving the most pronounced effects. In this regime, the intermediate information sources X and Y which are activated by the source S with low strength, in return, activate target Z with moderate strength. Fig. 6(c) presents the profile of  $\Delta I_{IM-DM}^{Add}(z; x, y)$  contributing maximum effective redundancy  $I_{ER}$ , where S interacts with X and Y weakly and so does both X and Y with Z. In this respect, we restate that the strength of activation is determined by the parameters  $K_1, K_2, K_3$  and,  $K_4$ . To be specific, by using  $K_1 = K_2 = 10 - 90$  and  $K_3 = K_4 = 100 - 900$  (all in molecules/V with  $V$  being the unit effective cellular volume)<sup>86</sup>, the nonlinear regulatory functions ( $s^n / (K_1^n + s^n)$ ,  $s^n / (K_2^n + s^n)$ ,  $x^n / (K_3^n + x^n)$  and,  $y^n / (K_4^n + y^n)$ ) in the production terms for X, Y and, Z, respectively, take numerical values in the range of 0.1 (weak activation) - 0.5 (moderate activation) at steady state.

The maps in Fig. 6(a,b,c) show that, with decreasing strength of activation of the intermediate X and Y by S and

by increasing the activation strength of Z by X and Y, the system acquires more redundancy for the BM-DM and the IM-DM-Mult as the case may be. For IM-DM-Add, the system chooses a decrease in the activation strength of Z by X and Y, to increase effective redundancy  $I_{ER}$  while, still holding weak interaction of S with X and Y. Here we redirect our attention to Fig. 2(a,b,c) where we have observed that SNR, the metric for fidelity in information processing,<sup>26</sup> increases with increasing effective redundancy  $I_{ER}$ . Keeping these points in mind, we propose that under weak activation levels of X and Y (i.e. low steady-state values of the nonlinear terms  $s^n/(K_1^n + s^n)$ , etc.) along with, either moderate activation levels of the target Z for multiplicative signal integration mechanism (i.e. moderate steady-state values of the nonlinear terms  $x^n/(K_3^n + x^n)$ , etc.) or weak activation levels of the target Z for additive signal integration mechanism (i.e. low steady-state values of the nonlinear terms  $x^n/(K_3^n + x^n)$ , etc.) maximum level of effective redundancy is likely to be selected naturally by incorporating suitable mutations. Therefore, noise minimizing biological motifs will eventually favor regulation of the above-mentioned strengths for biochemical species S, X, Y and Z.

One can find a similar situation in case of regulatory DNA sequence motifs where for a single transcription factor, there exist more than one operators with varying affinity. This phenomenon has been ascribed to the evolutionary tuning of the binding affinities so that the regulated gene can be made maximally functional. Here, one should keep in mind that these sequences are constantly exposed to simultaneous forces of natural selection and mutation. In essence, this links the genotype which is acted upon by mutation and, the phenotype which is selected if deemed fit in the backdrop of environmental changes<sup>87</sup>. Our predictions find resonance in the fact that high sequence specificity may be harmful to the transcription control network in the face of deleterious mutation. The system also keeps a check on the weaker end of specificity spectrum to avoid spurious interactions. This trade-off essentially provides the required robustness in the control network<sup>88</sup>.

#### D. Parametric dependence of net synergy contributions of different sub-motifs reveals the corresponding noise-tolerant sub-motif

To capture how the bifurcation and integration sub-motifs perform relative to each other in terms of their individual net synergy contributions, we show  $\Delta I_{IM-DM}^{Mult}(z; x, y) - \Delta I_{BM-DM}(s; x, y)$  as a function of  $\mu_x$  and  $\mu_y$  for  $\mu_s = 0.1 \text{ min}^{-1}$ ,  $\mu_s = 0.5 \text{ min}^{-1}$  and,  $\mu_s = 1 \text{ min}^{-1}$  in Fig. 7(a-c), respectively, within multiplicative integration scheme. The bifurcation sub-motif dominates in all of these landscapes which are negatively valued in most of the parts. The domain with maximum negativity, shifts higher up the diagonal ( $\mu_x = \mu_y$ ), as  $\mu_s$  increases from  $0.1 \text{ min}^{-1}$  to  $1 \text{ min}^{-1}$ . The contribution from the integration sub-motif dominates mainly along the region where any one of the tuning parameters ( $\mu_x$  or  $\mu_y$ ) is small in comparison with its counterpart while the remaining one scans its full range. As  $\mu_s$  increases, the relative contribution made by the integration sub-motif increases.

In support of the difference in the net synergy shown in Fig. 7(a-c), we now look at the difference in the SNR-s of the sub-motifs due to multiplicative integration scheme. The panels of Fig. 7(d-f), depict the corresponding variation in the difference between SNR-s of integration and bifurcation sub-motifs, i.e.  $\text{SNR}_{IM-DM}^{Mult} - \text{SNR}_{BM-DM}$  with  $\mu_s$  taking values of  $0.1 \text{ min}^{-1}$ ,  $0.5 \text{ min}^{-1}$  and,  $1 \text{ min}^{-1}$ , respectively. For computing  $\text{SNR}_{BM-DM}$  and  $\text{SNR}_{IM-DM}^{Mult}$ , we have considered the signaling branches  $S \rightarrow X$  and  $X \rightarrow Z$ , respectively. We note that with  $\mu_s = 0.1 \text{ min}^{-1}$ , the map consists of both positive and negative valued domains. In the positive region, the IM-DM has higher fidelity than the BM-DM whereas, for some specific combinations of the tuning parameters, the BM-DM overpowers the IM-DM, in its efficiency in high fidelity information processing, thereby creating a negatively valued region in this map. As  $\mu_s$  increases, the IM-DM takes control over the entire  $(\mu_x, \mu_y)$  parameter space but the difference between the two SNR-s gradually decreases. This analysis graphically marks different regions where particular sub-motif plays the leading role compared to its counterpart in increasing the fidelity in information transmission.

The two branches of both bifurcation and integration sub-motifs become identical when X and Y relax identically ( $\mu_x = \mu_y$ ). Under such a condition, where the two pathways namely  $S \rightarrow X \rightarrow Z$  and,  $S \rightarrow Y \rightarrow Z$  are mirror images of each other, we explored in Fig. 8(a-f) how the differences in between the net synergy-s and SNR-s of sub-motifs respond to change in integration logic. The first observation is that the net synergy differences are mostly negatively constrained while SNR differences are mostly positively constrained. However, for low  $\mu_s$  and for additive integration scheme these metrics span in both positive and negative spaces. For all strengths of the signal, it is observed that multiplicative integration gives more negative net synergy difference than additive integration. While for SNR differences, multiplicative integration contributes more positively than its additive counterpart. Two things, in particular, are worth mentioning. Mechanism wise, additive integration is seen to be spanning both positive and negative domains of the net synergy difference and SNR difference. The gap between contributions from multiplicative and additive mechanisms is the largest among all for the low  $\mu_s$  case. This type of computational investigation scanning different regimes of the net synergy and SNR may be helpful while constructing synthetic biological circuits which often implement logical computations in decision making processes<sup>62</sup>. After looking at the strong and weak regimes

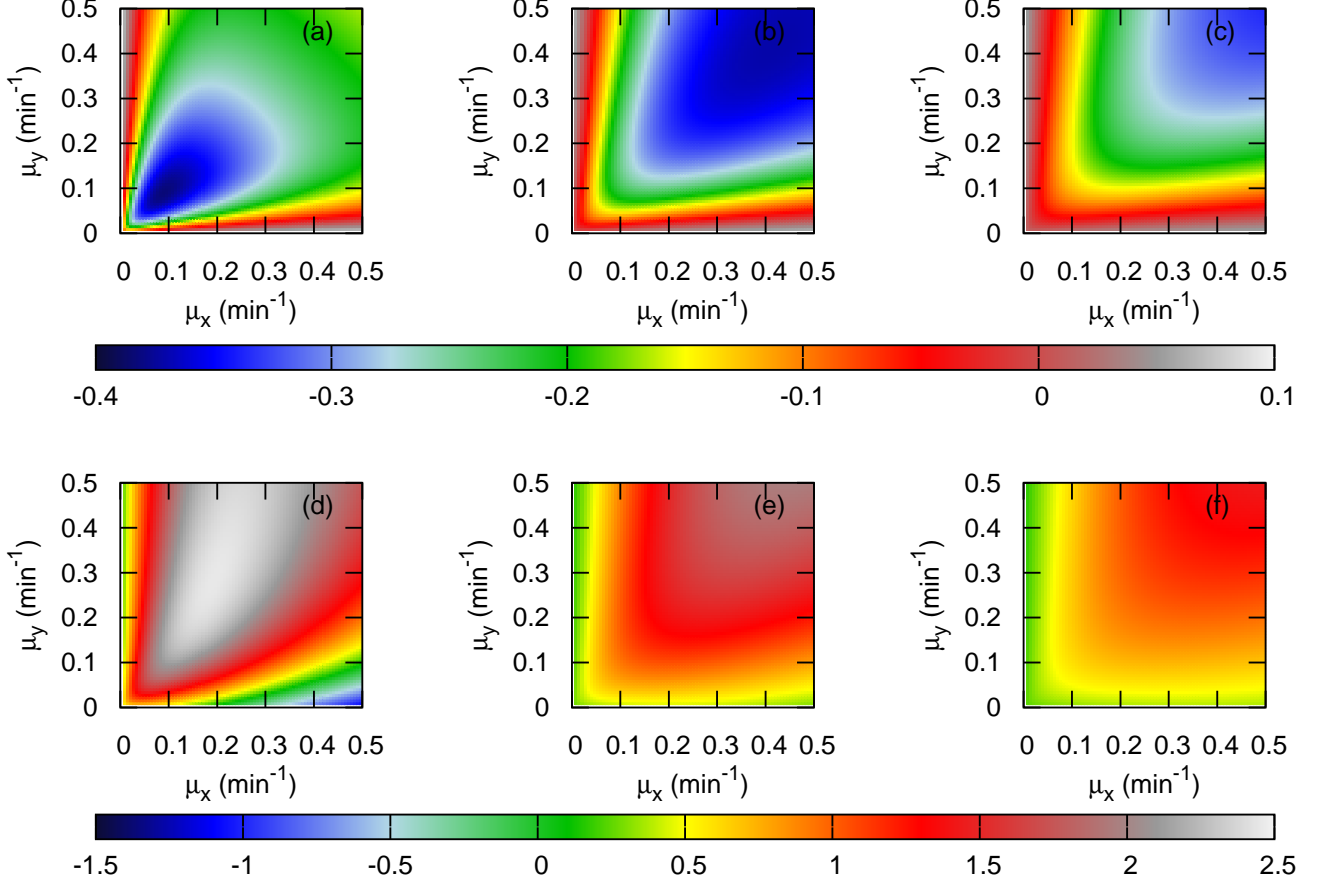


FIG. 7. Panels (a)-(c) depict  $\Delta I_{IM-DM}^{Mult}(z; x, y) - \Delta I_{BM-DM}(s; x, y)$  (in bits) as functions of  $\mu_x$  and  $\mu_y$  for  $\mu_s = 0.1, 0.5$  and,  $1 \text{ min}^{-1}$ , respectively. Similarly, panels (d)-(f) show  $\text{SNR}_{IM-DM}^{Mult} - \text{SNR}_{BM-DM}$  for  $\mu_s = 0.1, 0.5$  and,  $1 \text{ min}^{-1}$ , respectively.  $\text{SNR}_{BM-DM}$  and  $\text{SNR}_{IM-DM}^{Mult}$  are computed considering the signaling pathways  $S \rightarrow X$  and  $X \rightarrow Z$ , respectively. The theoretical expressions are obtained using constant populations (at steady state) of the biochemical species:  $\langle s \rangle = 10$ ,  $\langle x \rangle = 100$ ,  $\langle y \rangle = 100$  and,  $\langle z \rangle = 100$  all in molecules/ $V$  with  $V$  being the unit effective cellular volume. The expressions for the rate parameters are  $k_s = \mu_s \langle s \rangle$ ,  $k_x = \mu_x \langle x \rangle ((K_1^n + \langle s \rangle^n) / \langle s \rangle^n)$ ,  $k_y = \mu_y \langle y \rangle ((K_2^n + \langle s \rangle^n) / \langle s \rangle^n)$  and,  $k'_z = \mu_z \langle z \rangle ((K_3^n + \langle x \rangle^n) / \langle x \rangle^n) ((K_4^n + \langle y \rangle^n) / \langle y \rangle^n)$ . We have kept  $K_1 = K_2 = 90$ ,  $K_3 = K_4 = 100$  all in molecules/ $V$  with  $V$  being the unit effective cellular volume,  $\mu_z = 5 \text{ min}^{-1}$  and,  $n = 1$  throughout to generate the theoretical profiles.

and corresponding transitions, one may infer biologically plausible parameter sets with which synthetic circuits can be constructed to achieve specific goals, e.g. large net synergy and SNR differences. After that, the predictions can be tested against the output data generated through real experiments.

#### IV. CONCLUSION

To summarize, we have developed an information-theoretic characterization of DM using the formalism of PID. To know how much predictive power one biochemical component has about others, we have chosen the metric of net synergy that takes care of synergy, redundancy and, information independence. We have identified two sub-motifs namely the signal bifurcation motif and the signal integration motif out of the whole motif, i.e. the DM. From the set of Langevin equations, using LNA and after that Lyapunov equation at steady state we obtained the analytic expressions for the second moments of the Gaussian random variables. These variables represent different biochemical species of the network. The generic regulatory functions have been chosen to be nonlinear which is typically the case in real biological systems. In our analysis, we investigate the effect of the relaxation time scale on the information transmission in network motifs. It is important to note that a slower downstream species fails to sense the faster

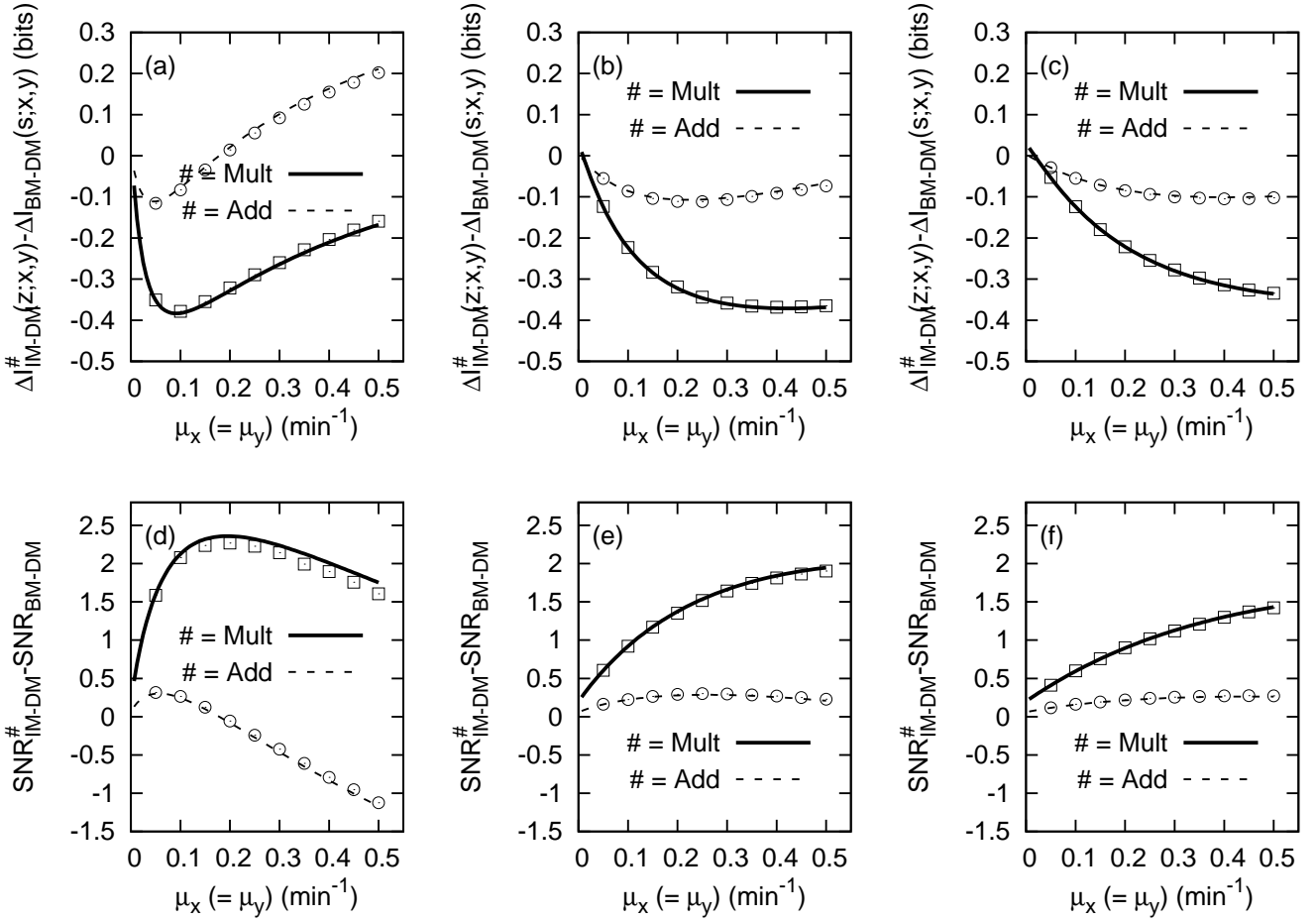


FIG. 8. Panels (a)-(c) depict  $\Delta I_{IM-DM}^{Mult}(z;x,y) - \Delta I_{BM-DM}(s;x,y)$  and  $\Delta I_{IM-DM}^{Add}(z;x,y) - \Delta I_{BM-DM}(s;x,y)$  (in bits) as functions of  $\mu_x (= \mu_y)$  for  $\mu_s = 0.1, 0.5$  and,  $1 \text{ min}^{-1}$ , respectively. Similarly, panels (d)-(f) show  $\text{SNR}_{IM-DM}^{Mult} - \text{SNR}_{BM-DM}$  and  $\text{SNR}_{IM-DM}^{Add} - \text{SNR}_{BM-DM}$  for  $\mu_s = 0.1, 0.5$  and,  $1 \text{ min}^{-1}$ , respectively.  $\text{SNR}_{BM-DM}$  and  $\text{SNR}_{IM-DM}$  ( $\text{SNR}_{IM-DM}^{Add}$ ) are computed considering the signaling pathways  $S \rightarrow X$  and  $X \rightarrow Z$ , respectively. The lines are due to analytical results and the symbols represent numerical data generated using Gillespie's algorithm<sup>77,78</sup> with an ensemble averaging over  $10^6$  independent time series. The expressions are obtained using constant populations (at steady state) of the biochemical species:  $\langle s \rangle = 10$ ,  $\langle x \rangle = 100$ ,  $\langle y \rangle = 100$  and,  $\langle z \rangle = 100$  all in molecules/ $V$  with  $V$  being the unit effective cellular volume. The expressions for the rate parameters are  $k_s = \mu_s \langle s \rangle$ ,  $k_x = \mu_x \langle x \rangle ((K_2^n + \langle s \rangle^n) / \langle s \rangle^n)$ ,  $k_y = \mu_y \langle y \rangle ((K_2^n + \langle s \rangle^n) / \langle s \rangle^n)$ ,  $k_z = \mu_z \langle z \rangle (\frac{\langle x \rangle^n}{K_3^n + \langle x \rangle^n} + \frac{\langle y \rangle^n}{K_4^n + \langle y \rangle^n})^{-1}$  and,  $k'_z = \mu_z \langle z \rangle ((K_3^n + \langle x \rangle^n) / \langle x \rangle^n) ((K_4^n + \langle y \rangle^n) / \langle y \rangle^n)$ . We have kept  $K_1 = K_2 = 90$ ,  $K_3 = K_4 = 100$  all in molecules/ $V$  with  $V$  being the unit effective cellular volume,  $\mu_z = 5 \text{ min}^{-1}$  and,  $n = 1$  throughout to generate the profiles.

upstream species and thus, information propagation is hindered in the channel. This study attempts to depict the effect of variation in relaxation time scale in the net synergy landscape. Effective redundancy is lowered whenever upstream species fluctuates on a faster time scale compared to the downstream species. Apart from the time scales, signal integration mechanisms were observed to play a definitive role to nurture the net synergy. Our computations reveal that SNR in the DM increases with effective redundancy  $I_{ER}$  for both signal integration logic.

Our study also uncovers the physical reason behind the creation of effective redundancy  $I_{ER}$  in the net synergy profile. We observe only effective synergy  $I_{ES}$  in the integration motif whose two signal integrating branches are architecturally disjoint from above, i.e. having no common source of fluctuations. Therefore, we are led to speculate that effective redundancy arises out of information sharing between different target nodes of the network, caused by a common source of fluctuations. Multiplicative integration of signal at the output is observed to generate more  $I_{ER}$  than additive integration in IM-DM. In an IM, multiplicative integration logic produces more  $I_{ES}$  than its additive counterpart.

There are indications emanating from variations of the net synergy as a function of various activation coefficients



that biological motifs with better noise handling capabilities will prefer weak activation for intermediate information nodes and moderate activation for the final downstream target species for multiplicative integration scheme. For additive integration logic, the final downstream target also needs to be weakly activated by the intermediates which themselves are weakly activated by the source.

We quantified the relative information processing strengths of the BM-DM and, IM-DM operating under low, medium and, high relaxation frequency of the signal with both additive and multiplicative integration logic. The related maps portraying the interplay of SNR-s of the two sub-motifs, under similar parametric conditions in the  $\mu_x, \mu_y$  domain help us to identify regions where specific sub-motifs contribute more towards high fidelity information transmission. While constructing synthetic biological logic circuits, one can easily select plausible parameter sets generated in these observations to achieve the desirable magnitude of net synergy and SNR. By durability and performance of these artificially constructed biological motifs, one can positively infer why only specific types of signal processing motifs and not all, are abundant in nature. These are highly interesting queries of evolutionary importance, leading to better understanding of functionality in relation with the architecture of living organisms.

In a nutshell, we investigated the connection between the emergence of effective synergy and effective redundancy and, the architectural or topological features of the diamond motif and its sub-motifs. For this purpose, we quantified the net synergy in our information-theoretic study. Our generalized analysis employing a biologically relevant model and parameters presents key concepts and adds novelty to the current understanding of information processing in a diamond motif. In future work, this information-theoretic framework as presented in this communication has enormous scope to reveal novel findings in other abundant network motifs. Eventually, it may lead towards the discovery of some unifying physical principles governing diversified biological systems constituted across length scales and operating across time scales.

## ACKNOWLEDGMENTS

Ayan Biswas is thankful to Bose Institute, Kolkata for a research fellowship. Financial support from the Council of Scientific and Industrial Research (CSIR), India [01(2771)/14/EMR-II] is thankfully acknowledged.

## Appendix A: The bifurcation motif

For a bifurcation motif, one needs to consider the dynamics of only S, X and, Y as expressed with the following set of Langevin equations

$$\begin{aligned}\frac{ds}{dt} &= f_s(s) - \mu_s s + \xi_s(t), \\ \frac{dx}{dt} &= f_x(s, x) - \mu_x x + \xi_x(t), \\ \frac{dy}{dt} &= f_y(s, y) - \mu_y y + \xi_y(t).\end{aligned}$$

The corresponding Jacobian obtained from linearizing this set is as follows:

$$\mathbf{J} = \begin{pmatrix} f'_{s,s} - \mu_s & 0 & 0 \\ f'_{x,s} & f'_{x,x} - \mu_x & 0 \\ f'_{y,s} & 0 & f'_{y,y} - \mu_y \end{pmatrix},$$

where  $f'_{s,s} \equiv f'_{s,s}(\langle s \rangle)$ ,  $f'_{x,s} \equiv f'_{x,s}(\langle s \rangle, \langle x \rangle)$ ,  $f'_{x,x} \equiv f'_{x,x}(\langle s \rangle, \langle x \rangle)$ ,  $f'_{y,s} \equiv f'_{y,s}(\langle s \rangle, \langle y \rangle)$  and,  $f'_{y,y} \equiv f'_{y,y}(\langle s \rangle, \langle y \rangle)$ . Here,  $\langle \dots \rangle$  denotes the steady state ensemble average and  $f'_{s,s}(\langle s \rangle)$  symbolically means that the regulatory function  $f_s$  has been differentiated with respect to  $s$  and evaluated at  $\langle s \rangle$  and so on. Using the Jacobian, we solve the Lyapunov

equation (6) and derive the analytic expressions for variance and covariance associated with the bifurcation motif.

$$\Sigma(s) = \frac{\alpha_s}{2(\mu_s - f'_{s,s})}, \quad (\text{A1})$$

$$\Sigma(s, x) = \frac{f'_{x,s} \Sigma(s)}{(\mu_s - f'_{s,s}) + (\mu_x - f'_{x,x})}, \quad (\text{A2})$$

$$\Sigma(s, y) = \frac{f'_{y,s} \Sigma(s)}{(\mu_s - f'_{s,s}) + (\mu_y - f'_{y,y})}, \quad (\text{A3})$$

$$\Sigma(x) = \frac{\alpha_x}{2(\mu_x - f'_{x,x})} + \frac{f'_{x,s} \Sigma(s, x)}{(\mu_x - f'_{x,x})}, \quad (\text{A4})$$

$$\Sigma(y) = \frac{\alpha_y}{2(\mu_y - f'_{y,y})} + \frac{f'_{y,s} \Sigma(s, y)}{(\mu_y - f'_{y,y})}, \quad (\text{A5})$$

$$\Sigma(x, y) = \frac{f'_{y,s} \Sigma(s, x) + f'_{x,s} \Sigma(s, y)}{(\mu_x - f'_{x,x}) + (\mu_y - f'_{y,y})}. \quad (\text{A6})$$

In our calculation, we have used  $f_s = k_s$ ,  $f_x = k_x(s^n/(K_1^n + s^n))$  and,  $f_y = k_y(s^n/(K_2^n + s^n))$ .  $\alpha_i \equiv \langle |\xi_i|^2 \rangle$  ( $i = s, x, y$ ) imply the ensemble averaged noise strengths evaluated at steady state.

## Appendix B: The integration motif

For the integration motif, only species X, Y and, Z are taken into account for which the Langevin description stands like the following:

$$\begin{aligned} \frac{dx}{dt} &= f_x(x) - \mu_x x + \xi_x(t), \\ \frac{dy}{dt} &= f_y(y) - \mu_y y + \xi_y(t), \\ \frac{dz}{dt} &= f_z(x, y, z) - \mu_z z + \xi_z(t). \end{aligned}$$

with the Jacobian,

$$\mathbf{J} = \begin{pmatrix} f'_{x,x} - \mu_x & 0 & 0 \\ 0 & f'_{y,y} - \mu_y & 0 \\ f'_{z,x} & f'_{z,y} & f'_{z,z} - \mu_z \end{pmatrix}.$$

Here  $f'_{x,x} \equiv f'_{x,x}(\langle x \rangle)$ ,  $f'_{y,y} \equiv f'_{y,y}(\langle y \rangle)$ ,  $f'_{z,x} \equiv f'_{z,x}(\langle x \rangle, \langle y \rangle, \langle z \rangle)$ ,  $f'_{z,y} \equiv f'_{z,y}(\langle x \rangle, \langle y \rangle, \langle z \rangle)$  and,  $f'_{z,z} \equiv f'_{z,z}(\langle x \rangle, \langle y \rangle, \langle z \rangle)$ . As in the previous case  $\langle \dots \rangle$  denotes a steady state ensemble average and  $f'_{x,x}(\langle x \rangle)$  symbolically means that the regulatory function  $f_x$  has been differentiated with respect to  $x$  and evaluated at  $\langle x \rangle$ , and so on. Solving the corresponding Lyapunov equation (6) at steady state yields expressions of the second moments,

$$\Sigma(x) = \frac{\alpha_x}{2(\mu_x - f'_{x,x})}, \quad (\text{B1})$$

$$\Sigma(y) = \frac{\alpha_y}{2(\mu_y - f'_{y,y})}, \quad (\text{B2})$$

$$\Sigma(x, y) = 0, \quad (\text{B3})$$

$$\Sigma(x, z) = \frac{f'_{z,x} \Sigma(x)}{(\mu_x - f'_{x,x}) + (\mu_z - f'_{z,z})}, \quad (\text{B4})$$

$$\Sigma(y, z) = \frac{f'_{z,y} \Sigma(y)}{(\mu_y - f'_{y,y}) + (\mu_z - f'_{z,z})}, \quad (\text{B5})$$

$$\begin{aligned} \Sigma(z) &= \frac{\alpha_z}{2(\mu_z - f'_{z,z})} \\ &+ \frac{f'_{z,x} \Sigma(x, z) + f'_{z,y} \Sigma(y, z)}{(\mu_z - f'_{z,z})}. \end{aligned} \quad (\text{B6})$$

Here,  $f_x = k_x$ ,  $f_y = k_y$ ,  $f_z = k_z((x^n/(K_3^n + x^n)) + (y^n/(K_4^n + y^n)))$  (Additive integration),  $f_z = k'_z(x^n/(K_3^n + x^n))(y^n/(K_4^n + y^n))$  (Multiplicative integration) and,  $\alpha_i$ -s ( $i = x, y, z$ ) imply, as in the previous case, steady state ensemble averaged noise strengths of different biochemical species.

### Appendix C: The diamond motif

For a diamond motif where S, X, Y and, Z are all involved, the full set of Langevin equations are

$$\begin{aligned}\frac{ds}{dt} &= f_s(s) - \mu_s s + \xi_s(t), \\ \frac{dx}{dt} &= f_x(s, x) - \mu_x x + \xi_x(t), \\ \frac{dy}{dt} &= f_y(s, y) - \mu_y y + \xi_y(t), \\ \frac{dz}{dt} &= f_z(s, x, y, z) - \mu_z z + \xi_z(t).\end{aligned}$$

For the above-mentioned kinetics, the Jacobian becomes

$$\mathbf{J} = \begin{pmatrix} f'_{s,s} - \mu_s & 0 & 0 & 0 \\ f'_{x,s} & f'_{x,x} - \mu_x & 0 & 0 \\ f'_{y,s} & 0 & f'_{y,y} - \mu_y & 0 \\ f'_{z,s} & f'_{z,x} & f'_{z,y} & f'_{z,z} - \mu_z \end{pmatrix}.$$

Here,  $f'_{s,s} \equiv f'_{s,s}(\langle s \rangle)$ ,  $f'_{x,s} \equiv f'_{x,s}(\langle s \rangle, \langle x \rangle)$ ,  $f'_{x,x} \equiv f'_{x,x}(\langle s \rangle, \langle x \rangle)$ ,  $f'_{y,s} \equiv f'_{y,s}(\langle s \rangle, \langle y \rangle)$ ,  $f'_{y,y} \equiv f'_{y,y}(\langle s \rangle, \langle y \rangle)$ ,  $f'_{z,s} \equiv f'_{z,s}(\langle s \rangle, \langle x \rangle, \langle y \rangle, \langle z \rangle)$ ,  $f'_{z,x} \equiv f'_{z,x}(\langle s \rangle, \langle x \rangle, \langle y \rangle, \langle z \rangle)$ ,  $f'_{z,y} \equiv f'_{z,y}(\langle s \rangle, \langle x \rangle, \langle y \rangle, \langle z \rangle)$  and,  $f'_{z,z} \equiv f'_{z,z}(\langle s \rangle, \langle x \rangle, \langle y \rangle, \langle z \rangle)$ . The notations  $\langle \dots \rangle$ ,  $f'_{s,s}(\langle s \rangle)$ , etc. have the usual meaning as mentioned in the previous two cases. Again with the help

of the Lyapunov equation (6), we get the following analytic expressions for variance and covariance,

$$\Sigma(s) = \frac{\alpha_s}{2(\mu_s - f'_{s,s})}, \quad (\text{C1})$$

$$\Sigma(s, x) = \frac{f'_{x,s} \Sigma(s)}{(\mu_s - f'_{s,s}) + (\mu_x - f'_{x,x})}, \quad (\text{C2})$$

$$\Sigma(s, y) = \frac{f'_{y,s} \Sigma(s)}{(\mu_s - f'_{s,s}) + (\mu_y - f'_{y,y})}, \quad (\text{C3})$$

$$\Sigma(s, z) = \frac{f'_{z,s} \Sigma(s) + f'_{z,x} \Sigma(s, x) + f'_{z,y} \Sigma(s, y)}{(\mu_s - f'_{s,s}) + (\mu_z - f'_{z,z})}, \quad (\text{C4})$$

$$\Sigma(x) = \frac{\alpha_x}{2(\mu_x - f'_{x,x})} + \frac{f'_{x,s} \Sigma(s, x)}{(\mu_x - f'_{x,x})}, \quad (\text{C5})$$

$$\Sigma(y) = \frac{\alpha_y}{2(\mu_y - f'_{y,y})} + \frac{f'_{y,s} \Sigma(s, y)}{(\mu_y - f'_{y,y})}, \quad (\text{C6})$$

$$\Sigma(x, y) = \frac{f'_{x,s} \Sigma(s, y) + f'_{y,s} \Sigma(s, x)}{(\mu_x - f'_{x,x}) + (\mu_y - f'_{y,y})}, \quad (\text{C7})$$

$$\Sigma(x, z) = \frac{f'_{x,s} \Sigma(s, z) + f'_{z,s} \Sigma(s, x) + f'_{z,x} \Sigma(x) + f'_{z,y} \Sigma(x, y)}{(\mu_x - f'_{x,x}) + (\mu_z - f'_{z,z})}, \quad (\text{C8})$$

$$\Sigma(y, z) = \frac{f'_{y,s} \Sigma(s, z) + f'_{z,s} \Sigma(s, y) + f'_{z,y} \Sigma(y) + f'_{z,x} \Sigma(x, y)}{(\mu_y - f'_{y,y}) + (\mu_z - f'_{z,z})}, \quad (\text{C9})$$

$$\Sigma(z) = \frac{\alpha_z}{2(\mu_z - f'_{z,z})} + \frac{f'_{z,s} \Sigma(s, z) + f'_{z,x} \Sigma(x, z) + f'_{z,y} \Sigma(y, z)}{(\mu_z - f'_{z,z})}. \quad (\text{C10})$$

For diamond motif, the regulatory functions are chosen as,  $f_s = k_s$ ,  $f_x = k_x(s^n/(K_1^n + s^n))$ ,  $f_y = k_y(s^n/(K_2^n + s^n))$ ,  $f_z = k_z((x^n/(K_3^n + x^n)) + (y^n/(K_4^n + y^n)))$  (Additive integration),  $f_z = k'_z(x^n/(K_3^n + x^n))(y^n/(K_4^n + y^n))$  (Multiplicative integration) and  $\alpha_i$ -s ( $i = s, x, y, z$ ) stand for different steady state noise strengths obtained through ensemble averaging. We utilize these expressions of second moments (Eqs. C1-C10) to compute  $\Delta I_{BM-DM}(s; x, y)$  and  $\Delta I_{IM-DM}(z; x, y)$  (for additive and multiplicative integration scheme), as required.

<sup>1</sup>M. Thattai and A. van Oudenaarden, Proc. Natl. Acad. Sci. U.S.A. **98**, 8614 (2001).

<sup>2</sup>H. B. Fraser, A. E. Hirsh, G. Giaever, J. Kumm, and M. B. Eisen, PLoS Biol. **2**, e137 (2004).

<sup>3</sup>C. T. Bergstrom and M. Lachmann, *Shannon information and biological fitness* in *Information Theory Workshop* (IEEE, 2004).

<sup>4</sup>W. Bialek and S. Setayeshgar, Proc. Natl. Acad. Sci. U.S.A. **102**, 10040 (2005).

<sup>5</sup>B. Ghosh, R. Karmakar, and I. Bose, Phys Biol **2**, 36 (2005).

<sup>6</sup>S. F. Taylor, N. Tishby, and W. Bialek (2007), arXiv:0712.4382v1 [q-bio.PE].

<sup>7</sup>W. Bialek and S. Setayeshgar, Phys. Rev. Lett. **100**, 258101 (2008).

<sup>8</sup>G. Tkačik, C. G. Callan, and W. Bialek, Phys Rev E **78**, 011910 (2008).

<sup>9</sup>W. Bialek, *Biophysics: Searching for principles* (Princeton University Press, Princeton, 2012).

<sup>10</sup>C. G. Bowsler and P. S. Swain, Curr. Opin. Biotechnol. **28**, 149 (2014).

<sup>11</sup>A. Levchenko and I. Nemenman, Curr. Opin. Biotechnol. **28**, 156 (2014).

<sup>12</sup>S. S. Mc Mahon, A. Sim, S. Filippi, R. Johnson, J. Liepe, D. Smith, and M. P. Stumpf, Semin. Cell Dev. Biol. **35**, 98 (2014).

<sup>13</sup>J. Selimkhanov, B. Taylor, J. Yao, A. Pilko, J. Albeck, A. Hoffmann, L. Tsimring, and R. Wollman, Science **346**, 1370 (2014).

<sup>14</sup>D. Hathcock, J. Sheehy, C. Weisenberger, E. Ilker, and M. Hinczewski, IEEE Transactions on Molecular, Biological and Multi-Scale Communications **2**, 16 (2016).

<sup>15</sup>C. E. Shannon, Bell. Syst. Tech. J **27**, 379 (1948).

<sup>16</sup>T. M. Cover and J. A. Thomas, *Elements of Information Theory* (Wiley-Interscience, New York, 1991).

<sup>17</sup>D. J. C. MacKay, *Information Theory, Inference & Learning Algorithms* (Cambridge University Press, New York, 2002).

<sup>18</sup>A. Borst and F. E. Theunissen, Nat. Neurosci. **2**, 947 (1999).

<sup>19</sup>P. P. Mitra and J. B. Stark, Nature **411**, 1027 (2001).

<sup>20</sup>E. Ziv, I. Nemenman, and C. H. Wiggins, PLoS ONE **2**, e1077 (2007).

<sup>21</sup>I. Lestas, G. Vinnicombe, and J. Paulsson, Nature **467**, 174 (2010).

<sup>22</sup>F. Tostevin and P. R. ten Wolde, Phys. Rev. E **81**, 061917 (2010).

- <sup>23</sup>R. Cheong, A. Rhee, C. J. Wang, I. Nemenman, and A. Levchenko, *Science* **334**, 354 (2011).
- <sup>24</sup>G. Tkačik and A. M. Walczak, *J. Phys. Condens. Matter* **23**, 153102 (2011).
- <sup>25</sup>A. Rhee, R. Cheong, and A. Levchenko, *Phys Biol* **9**, 045011 (2012).
- <sup>26</sup>C. G. Bowsher, M. Voliotis, and P. S. Swain, *PLoS Comput. Biol.* **9**, e1002965 (2013).
- <sup>27</sup>L. S. Tsimring, *Rep. Prog. Phys.* **77**, 026601 (2014).
- <sup>28</sup>A. S. Hansen and E. K. O’Shea, *Elife* **4**, e06559 (2015).
- <sup>29</sup>R. Milo, S. Shen-Orr, S. Itzkovitz, N. Kashtan, D. Chklovskii, and U. Alon, *Science* **298**, 824 (2002).
- <sup>30</sup>F. Mancini, C. H. Wiggins, M. Marsili, and A. M. Walczak, *Phys. Rev. E* **88**, 022708 (2013).
- <sup>31</sup>W. Weaver, *Sci. Am.* **181**, 11 (1949).
- <sup>32</sup>U. Alon, *An Introduction to Systems Biology: Design Principles of Biological Circuits* (CRC Press, Boca Raton, 2006).
- <sup>33</sup>U. Alon, *Nat. Rev. Genet.* **8**, 450 (2007).
- <sup>34</sup>W. H. de Ronde, F. Tostevin, and P. R. ten Wolde, *Phys Rev E* **86**, 021913 (2012).
- <sup>35</sup>A. Cournac and J. A. Sepulchre, *BMC Syst Biol* **3**, 29 (2009).
- <sup>36</sup>E. Schneidman, W. Bialek, and M. J. Berry II, *J. Neurosci.* **23**, 11539 (2003).
- <sup>37</sup>A. B. Barrett, *Phys. Rev. E* **91**, 052802 (2015).
- <sup>38</sup>P. L. Williams and R. D. Beer (2010), arXiv: cs.IT/1004.2515.
- <sup>39</sup>N. Timme, W. Alford, B. Flecker, and J. M. Beggs, *J Comput Neurosci* **36**, 119 (2014).
- <sup>40</sup>L. Faes, D. Kugiumtzis, G. Nollo, F. Jurysta, and D. Marinazzo, *Phys Rev E* **91**, 032904 (2015).
- <sup>41</sup>L. Faes, D. Marinazzo, and S. Stramaglia, *Entropy* **19**, 408 (2017).
- <sup>42</sup>L. Faes, A. Porta, G. Nollo, and M. Javorka, *Entropy* **19**, 5 (2017).
- <sup>43</sup>L. Faes, A. Porta, and G. Nollo, *Entropy* **17**, 277 (2015).
- <sup>44</sup>N. Bertschinger, J. Rauh, E. Olbrich, J. Jost, and N. Ay, *Entropy* **16**, 2161 (2014).
- <sup>45</sup>V. Griffith and C. Koch, in *Guided self-organization: Inception, Emergence, complexity and computation*, edited by M. Prokopenko (Springer, Berlin, 2014), vol. 9, pp. 159–190.
- <sup>46</sup>M. Harder, C. Salge, and D. Polani, *Phys Rev E* **87**, 012130 (2013).
- <sup>47</sup>M. Wibrall, V. Priesemann, J. W. Kay, J. T. Lizier, and W. A. Phillips, *Brain Cogn* **112**, 25 (2017).
- <sup>48</sup>T. J. Gawne and B. J. Richmond, *J. Neurosci.* **13**, 2758 (1993).
- <sup>49</sup>S. Panzeri, S. R. Schultz, A. Treves, and E. T. Rolls, *Proc. Biol. Sci.* **266**, 1001 (1999).
- <sup>50</sup>N. Brenner, S. P. Strong, R. Koberle, W. Bialek, and R. R. de Ruyter van Steveninck, *Neural Comput* **12**, 1531 (2000).
- <sup>51</sup>F. Montani, R. A. A. Ince, R. Senatore, E. Arabzadeh, M. E. Diamond, and S. Panzeri, *Philos Trans A* **367**, 3297 (2009).
- <sup>52</sup>C. E. Shannon and W. Weaver, *The mathematical theory of communication* (Urbana: University of Illinois Press, 1963).
- <sup>53</sup>A. Biswas and S. K. Banik, *Phys Rev E* **93**, 052422 (2016).
- <sup>54</sup>G. Tkačik, A. M. Walczak, and W. Bialek, *Phys Rev E* **80**, 031920 (2009).
- <sup>55</sup>G. Rodrigo and J. F. Poyatos, *PLoS Comput. Biol.* **12**, e1005156 (2016).
- <sup>56</sup>A. Rhee, R. Cheong, and A. Levchenko, *Proc. Natl. Acad. Sci. U.S.A.* **111**, 17330 (2014).
- <sup>57</sup>F. J. Bruggeman, N. Blüthgen, and H. V. Westerhoff, *PLoS Comput. Biol.* **5**, e1000506 (2009).
- <sup>58</sup>M. Hinczewski and D. Thirumalai, *Phys. Rev. X* **4**, 041017 (2014).
- <sup>59</sup>A. K. Maity, P. Chaudhury, and S. K. Banik, *PLoS ONE* **10**, e0123242 (2015).
- <sup>60</sup>Y. Setty, A. E. Mayo, M. G. Surette, and U. Alon, *Proc. Natl. Acad. Sci. U.S.A.* **100**, 7702 (2003).
- <sup>61</sup>A. E. Mayo, Y. Setty, S. Shavit, A. Zaslaver, and U. Alon, *PLoS Biol.* **4**, e45 (2006).
- <sup>62</sup>R. Silva-Rocha and V. de Lorenzo, *FEBS Lett.* **582**, 1237 (2008).
- <sup>63</sup>W. H. de Ronde, F. Tostevin, and P. R. ten Wolde, *Phys. Rev. E* **82**, 031914 (2010).
- <sup>64</sup>S. Tănase-Nicola, P. B. Warren, and P. R. ten Wolde, *Phys. Rev. Lett.* **97**, 068102 (2006).
- <sup>65</sup>P. B. Warren, S. Tănase-Nicola, and P. R. ten Wolde, *J. Chem. Phys.* **125**, 144904 (2006).
- <sup>66</sup>A. K. Maity, A. Bandyopadhyay, P. Chaudhury, and S. K. Banik, *Phys. Rev. E* **89**, 032713 (2014).
- <sup>67</sup>R. Grima, *Phys. Rev. E* **92**, 042124 (2015).
- <sup>68</sup>M. B. Elowitz, A. J. Levine, E. D. Siggia, and P. S. Swain, *Science* **297**, 1183 (2002).
- <sup>69</sup>J. Paulsson, *Nature* **427**, 415 (2004).
- <sup>70</sup>J. Elf and M. Ehrenberg, *Genome Res.* **13**, 2475 (2003).
- <sup>71</sup>N. G. van Kampen, *Stochastic Processes in Physics and Chemistry, 3rd ed.* (North-Holland, Amsterdam, 2007).
- <sup>72</sup>F. Tostevin and P. R. ten Wolde, *Phys. Rev. Lett.* **102**, 218101 (2009).
- <sup>73</sup>L. Bintu, N. E. Buchler, H. G. Garcia, U. Gerland, T. Hwa, J. Kondev, and R. Phillips, *Curr. Opin. Genet. Dev.* **15**, 116 (2005).
- <sup>74</sup>G. Tkačik, T. Gregor, and W. Bialek, *PLoS ONE* **3**, e2774 (2008).
- <sup>75</sup>A. M. Walczak, G. Tkačik, and W. Bialek, *Phys Rev E* **81**, 041905 (2010).
- <sup>76</sup>G. Tkačik, C. G. Callan, and W. Bialek, *Proc. Natl. Acad. Sci. U.S.A.* **105**, 12265 (2008).
- <sup>77</sup>D. T. Gillespie, *J. Comp. Phys.* **22**, 403 (1976).
- <sup>78</sup>D. T. Gillespie, *J. Phys. Chem.* **81**, 2340 (1977).
- <sup>79</sup>P. S. Swain, *J. Mol. Biol.* **344**, 965 (2004).
- <sup>80</sup>P. Mehta, S. Goyal, and N. S. Wingreen, *Mol. Syst. Biol.* **4**, 221 (2008).
- <sup>81</sup>J. Keizer, *Statistical Thermodynamics of Nonequilibrium Processes* (Springer-Verlag, Berlin, 1987).
- <sup>82</sup>J. Paulsson, *Phys Life Rev* **2**, 157 (2005).
- <sup>83</sup>I. Golding, J. Paulsson, S. M. Zawilski, and E. C. Cox, *Cell* **123**, 1025 (2005).
- <sup>84</sup>F. Montani, A. Kohn, M. A. Smith, and S. R. Schultz, *J. Neurosci.* **27**, 2338 (2007).
- <sup>85</sup>L. Montangie and F. Montani, *Phys Rev E* **94**, 042303 (2016).
- <sup>86</sup>N. E. Buchler and F. R. Cross, *Mol. Syst. Biol.* **5**, 272 (2009).
- <sup>87</sup>U. Gerland and T. Hwa, *J. Mol. Evol.* **55**, 386 (2002).
- <sup>88</sup>A. M. Sengupta, M. Djordjevic, and B. I. Shraiman, *Proc. Natl. Acad. Sci. U.S.A.* **99**, 2072 (2002).